This article has been accepted for publication in a future issue of this journal, but has not been fully edited. Content may change prior to final publication. Citation information: DOI 10.1109/TVT.2020.3037212, IEEE Transactions on Vehicular Technology

A Novel Atmosphere-informed Data-driven Predictive Channel Modeling for B5G/6G Satellite-terrestrial Wireless Communication Systems at Q-band

Lu Bai, *Member, IEEE*, Qian Xu, Shangbin Wu, Spiros Ventouras, and George Goussetis, *Senior Member, IEEE*

***Abstract*—This paper proposes a novel atmosphere-informed predictive satellite channel model for beyond the fifth-generation (B5G)/the sixth-generation (6G) satellite-terrestrial wireless communication systems at Q-band to model/predict channel attenuation at any specific time. The proposed channel model is a data-driven model based on either of two deep learning networks, i.e., multi-layer perceptron (MLP) and long short-term memory (LSTM). The accuracy of the proposed channel model is measured by cumulative density function (CDF) of absolute error and mean square error (MSE) between modeled/predicted and measured channel attenuation. The complexity of the proposed channel model is assessed by the training time, loading time, and test time of deep learning networks. To further improve the accuracy of the proposed channel model, weather classification is developed at the stage of database construction. Based on our established channel and weather measurement campaign, the performance of the proposed data-driven channel model based on different deep learning networks, e.g., MLP and LSTM, with or without the weather classification is investigated and analyzed comprehensively. Finally, the close agreement is achieved between the channel attenuation modeled/predicted from the proposed atmosphere-informed predictive satellite channel model and the one from real channel measurements, verifying the utility of proposed channel model.**

***Index Terms*—Channel modeling and measurement, B5G/6G satellite-terrestrial wireless communications, Q-band, data-driven, deep learning networks.**

I. Introduction

BY the fourth quarter of 2019, the number of mobile subscription reached 7.9 billion globally [1]. It is exciting that mobile technologies have become not only a connection between people, but also an accelerator of innovation. To let mobile technologies revolutionize every aspect in every one's daily life, two emerging issues are increasingly attracting attention from both industry and academia. The first one is the unprecedented growth of mobile data traffic. According to [1], there was a 49% growth of mobile data traffic within the one year period between Q4 2018 and Q4 2019. This growth rate is challenging the speed of technology evolution, the conventional business model of mobile network operators, and the environmental friendliness of large-scale network deployments. The second one is the connectivity gap between developed economies and underdeveloped economies. Although it is reported that more than half of the population have access to mobile connections, more than 3.5 billion people in underdeveloped countries remain unconnected to the internet [2]. The evolution of the fifth-generation (5G) mobile networks or even beyond 5G (B5G) and the sixth-generation (6G) mobile networks is targeting to address both of the above-mentioned issues [3]. One key candidate technology is the integration of satellite communications and 5G. To enable seamless transition between them, an accurate and easy-to-use satellite-terrestrial channel attenuation model is essential.

There are extensive satellite channel studies in the literature, covering frequency bands including UHF-band (300-3000 MHz) [4], L-band (1-2 GHz) [5], S-band (2-4 GHz) [6], X-band (8-12 GHz) [7], Ku-band (12-18 GHz) [7]–[8], K-band (18-26 GHz) [9], Ka-band (26-40 GHz) [10]–[12]. The research on satellite communication channel models at higher frequency bands, such as Q-band (33-50 GHz) and V-band (50-75 GHz) are less studied [13]–[16]. Recently, Q/V-band attracts a lot of attention because its high data throughput is beneficial to the transition from broadcast to broadband services in B5G and 6G satellite-terrestrial wireless communication systems. Moreover, Q/V-band are expected to be used for the feeder link of B5G and 6G satellite-terrestrial wireless communication systems to free Ka-band for revenue generating user links and reduce the per bit cost of the ground segment [17]. The channel characteristics of satellite channel model at higher frequency bands are different from that at low frequency band [18]–[20], so the channel models at lower frequency band [4]–[12] cannot be directly used for satellite channels at Q/V-bands. Therefore, an accurate yet easy-to-use satellite channel model which can describe channel characteristics at Q-band is necessary for the proper design and development of B5G and 6G satellite-terrestrial wireless communication systems [21]. However, currently the satellite

This work was supported in part by the National Natural Science Foundation of China (Grant No. 62001018).

L. Bai is with the School of Cyber Science and Technology, Beihang University, Beijing, 100191, China (e-mail:lu_bai@buaa.edu.cn).

Q. Xu is with the School of Computer Science and Technology, Jilin University, Changchun, Jilin, 130012, China (e-mail: quincyxu@hotmail.com).

S. Wu is with Samsung R&D Institute UK, Staines-upon-Thames, TW18 4QE, U.K. (e-mail: shangbin.wu@samsung.com).

S. Ventouras is with STFC Rutherford Appleton Laboratory, RAL Space, Oxford, OX11 0QX, U.K. (e-mail: spiros.ventouras@stfc.ac.uk).

G. Goussetis is with the Institute of Sensors, Signals and Systems, School of Engineering and Physical Sciences, Heriot-Watt University, Edinburgh, EH14 4AS, U.K. (e-mail: g.goussetis@hw.ac.uk).

This article has been accepted for publication in a future issue of this journal, but has not been fully edited. Content may change prior to final publication. Citation information: DOI 10.1109/TVT.2020.3037212, IEEE Transactions on Vehicular Technology

channel modeling at Q-band is still in the infancy stage. [13]–[15] presents the performance evaluation and analysis of fading estimation over Q/V-band satellite links, but they did not propose a complete channel model at Q-band. In [16], the authors proposed a three-dimensional channel model for satellite communications at Q-band in a high latitude, including the path loss, shadowing, and small-scale fading. This model is based on the stochastic channel modeling and cannot accurately model satellite channel attenuation at any specific time. Moreover, the limited opportunities to obtain satellite channel measurement data at Q-band leads to its channel modeling to be even more difficult, and thus slows down the development progress of Q-band channel modeling. Recently, [22] has discovered the correlation and relationship between the satellite channel attenuation at Q-band and atmosphere data. This preliminary investigation inspires us to use widely available atmosphere data, which is much easier to obtain than channel measurement data, to propose a new Q-band satellite channel modeling approach with the help of machine learning.

Importantly, the predictive ability of machine learning algorithm, i.e., multilayer perceptron (MLP) and long short-term memory (LSTM), enables predictive features of the new atmosphere data-based modeling approach. So far, conventional channel models can be classified as deterministic channel models, stochastic channel models, and machine learning-based channel models [23]. Neither of the aforementioned satellite channel models [4]–[12] can accurately model satellite channel attenuation at any specific time, which is necessary for efficient link adaptations including power control and adaptive coding and modulation (ACM) selection for satellite communications [24], [25]. Meanwhile, current channel models based on machine learning are all based on the channel propagation data obtained from real wireless channel measurement campaigns [26]. Because of the high cost of satellite channel measurement campaign at Q-band, the atmosphere data is much easier to obtain than the channel measurement data. A machine learning-based channel model with the help of the atmosphere data rather than the channel propagation data can relieve the difficult-to-obtain satellite channel measurement data at Q-band. Therefore proposing a new channel modeling approach based on atmosphere data, which can not only properly model Q-band satellite channel properties, but also predict channel attenuation at any interesting and specific time, is still an open area.

In this paper, to fill the aforementioned gap, we propose an atmosphere-informed data-driven predictive satellite channel model for B5G and 6G satellite-terrestrial wireless communication systems at Q-band based on two deep learning networks, i.e., MLP and LSTM. The main contributions of this paper are summarized as follows:

1) An atmosphere-informed data-driven predictive satellite channel model for B5G and 6G satellite-terrestrial wireless communication systems at Q-band is proposed in this paper. The proposed model can not only model Q-band channel characteristics based on atmosphere data, but also predict channel attenuation at any interesting and specific time. The term "channel prediction" refers to the ability of modeling channel attenuation at future time in advance. Therefore, both the terms "model" and "predict" are used in this paper to describe the proposed model's ability.
2) A new measurement campaign is built up at Chilbolton, Hampshire, UK, for training and validating the proposed data-driven channel model. The development measurement campaign can offer both the channel data at Q-band and the corresponding atmosphere data at the same time.
3) For further improving the accuracy of the proposed channel model, the weather classification during the process of the database construction is developed for the first time. Based on the established measurement campaign, the impact of the developed weather classification on the proposed data-driven channel model is fully analyzed and discussed, demonstrating the importance and necessity of the weather classification.
4) Based on the established measurement campaign at Chilbolton, UK, the utility of the proposed channel model is validated by the close agreement between the channel attenuation modeled/predicted from the proposed channel model and the one from real channel measurements. Moreover, the accuracy and complexity of the proposed channel model based on different deep learning networks, e.g., MLP and LSTM, with or without the weather classification are completely analyzed and discussed. Some interesting observations and useful conclusions are found, which are important and useful for the better design of B5G/6G satellite terrestrial wireless communication systems.

The rest of the paper is organized as follows. In Section II, the satellite communication system at Q-band and atmosphere measurement system are shown. In Section III, the atmosphere-informed data-driven predictive satellite channel model based on MLP is proposed. The weather classification and performance analysis are also shown. In Section IV, the atmosphere-informed data-driven predictive satellite channel model based on LSTM is shown. Its performance analysis is also investigated. In Section V, the atmosphere-informed data-driven predictive satellite channel model based on MLP and LSTM with weather classification are compared and discussed according to the trade-of between accuracy and complexity. Conclusions are given in Section VI.

Table I lists the abbreviations and their full names in this paper.

II. Measurement Systems and Weather Classification

A. Satellite channel attenuation measurements

The measurement campaign was conducted at Q-band (39.402 GHz) exploiting the Aldo Paraboni experimental payload on-board the commercial satellite Inmarsat-4A FA located at 25.0°E. The signal was received by a station mounted 10 m above rooftop located at Chilbolton, Hampshire, UK (51.1445°N, 1.4370°W). This measurement campaign has been operating since July 2016. In this paper, excess attenuation is our main focus and its behavior over time was recorded in the measurement campaign. As part of the

This article has been accepted for publication in a future issue of this journal, but has not been fully edited. Content may change prior to final publication. Citation information: DOI 10.1109/TVT.2020.3037212, IEEE Transactions on Vehicular Technology

TABLE I: Summary of abbreviations.

Full name	Abbreviation
Beyond the fifth-generation	B5G
Sixth-generation	6G
Multi-layer perceptron	MLP
Long short-term memory	LSTM
Cumulative density function	CDF
Mean square error	MSE
Adaptive coding and modulation	ACM
Rainfall drop count	RDC
Artificial neural network	ANN
Rectified linear unit	ReLU
Root-mean-square propagation	RMSProp
Recurrent neural network	RNN

measurement campaign, the excess attenuation under different weather condition was recorded. To eliminate the impact of ground equipment, the excess attenuation was extracted from the received signals by calculating the difference between the measured signal power and the power of a reference signal in clear sky.

B. Atmosphere measurements

To compare against weather conditions, the corresponding atmosphere data were also recorded. In order to improve the accuracy of proposed atmosphere-informed data-driven predictive satellite channel model, the satellite channel attenuation data and the corresponding atmosphere data are synchronized over time by seconds. The atmosphere data were collected using three instruments, including Campbell Scientific PWS100 present weather sensors, multiple raingauges, and meteorological sensors, in the Chilbolton Observatory, Hampshire, UK [27]–[29]. Fig. 1 (a) is the location of Chilbolton. Fig. 1 (b) is the Chilbolton Observatory [30].

These sensors and instruments were able to capture 14 measured parameters ranging from air temperature to rainfall drop count (RDC). A list of these atmosphere condition parameters are shown in Table II. There parameters will serve as inputs to the proposed channel attenuation model in later paragraphs.

III. Channel Model Based on MLP

A. System model

The artificial neural network (ANN) in this model is a MLP with 6 fully connection layers. The architecture parameters such as the learning rate, mini batch, epochs, and loss function, are adjusted to find the best performance. There are 16, 32, 64, 32, 16, and 1 neurons, respectively in each fully connection layer. The structure of this model is shown in Fig. 2. The loss function is applied to parameteric estimation. It is used to evaluate the performance of model by comparing the predicted value with the expected value. In this model, the mean square error (MSE) is used as the loss function. It is the average value

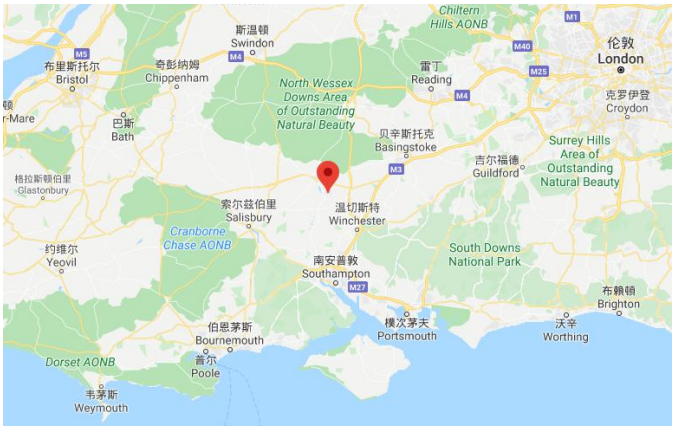

(a) The location of Chilbolton.

(b) The Chilbolton Observatory.

Fig. 1: The photographs of Chilbolton Observatory.

TABLE II: Measured atmosphere parameters.

Parameter	Unit
Air temperature	K
Relative humidity	%
Rainfall rate	m/s
Visibility	m
Thickness of rainfall amount	m
Average particle diameter	mm
Average particle speed	m/s
RDC 1 within turf wall enclosure	count
RDC 2 on ground	count
RDC 3 from low rate raingauge on ground	count
Rainfall tip count	count
Barmetric pressure	Pa
Wind speed	m/s
Wind direction	degree

of squared distances between our target values and predicted values, and can be expressed as

$$R = \frac{\sum_{n=1}^{N}(y_n - y_n^{\mathrm{p}})^2}{N} \tag{1}$$

where N denotes the numbers of dataset, y_n denotes true value and y_n^p denotes predicted value, respectively. The optimizer is used to minimize the value of MSE through iterations using the training dataset. Rectified linear unit (ReLU) is used in our

This article has been accepted for publication in a future issue of this journal, but has not been fully edited. Content may change prior to final publication. Citation information: DOI 10.1109/TVT.2020.3037212, IEEE Transactions on Vehicular Technology

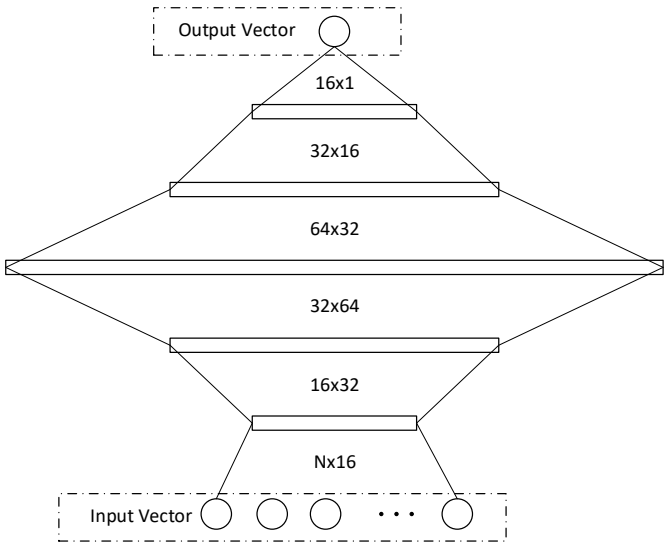

Fig. 2: The ANN architecture of proposed model for channel excess attenuation prediction.

model to accelerate the early stages of learning by providing positive inputs. ReLU is a popular activation function in deep learning, and could preserve information about relative intensities as information travels through multiple layers of feature detectors [31]. The learning rates for all the fully connection layers are set to 10^{-4} and divided by 10 every 100 epochs. The root-mean-square propagation (RMSProp) with the smooth factor of 10^{-6} and the momentum of 0.9 is applied to optimize the weights. The weight β is updated as below

$$\mathrm{E}[g^2]_t = 0.9\mathrm{E}[g^2]_{t-1} + 0.1g_t^2 \tag{2}$$

$$\beta_{t+1} = \beta_t - \frac{\eta}{\sqrt{\mathrm{E}[g^2]_t + \kappa}} g_t \tag{3}$$

where t denotes the iteration index, η denotes the learning rate, and κ denotes the smooth factor, respectively, g_t is the gradient of the current iteration t [32] [33]. The Glorot uniform initializer, which is also recognized as the Xavier uniform initializer, is applied to initialize the weights in each layer. Xavier uniform initializer is first proposed by Xavier Glorot and Yoshua Bengio in [34], and is widely used in the training deep feedforward neural networks. In order to make the information flow in the network more efficient, the variance of output of each layer should be equal as far as possible. A uniform distribution randomly within $[-\varepsilon, \varepsilon]$ was used to generate the weight where

$$\varepsilon = \sqrt{\frac{6}{\iota_{\mathrm{in}} + \iota_{\mathrm{out}}}} \tag{4}$$

where l_{in} and l_{out} are the numbers of input units and output units in the weight tensor. The neuron biases in all fully connection layers is initialized with the constant 0.

B. Weather classification and database description

According to our preliminary research on the correlation between the satellite channel attenuation at Q-band and atmosphere data [22], the rainfall amount has significant effect on the channel attenuation. Combined with the characteristic of ANN, this inspires us to exploit weather classification as prior information for improving the modeling/prediction performance of the proposed model.

To validate the performance of weather classification on the proposed atmosphere-informed data-driven predictive satellite channel model, a sunny database and a rainy database are built according to the thickness of rainfall amount from total samples. Meanwhile, the entire database comprises all samples. For a certain sample, if its thickness of rainfall amount is zero, this sample belongs to the sunny database, otherwise, this sample belongs to the rainy database. These databases are separated into training datasets, validation datasets, and testing datasets according to the proportion 60%, 15%, and 25%, respectively. In this paper, the proposed atmosphere-informed data-driven predictive satellite channel models trained by the entire database, sunny database, and rainy database are named as the general model, sunny model, and rainy model, respectively. In the same way, using the testing datasets of entire database, sunny database, and rainy database to test the prediction performance of channel models are named as the general prediction, sunny prediction, and rainy prediction, respectively. Therefore, based on a very simple inspection of the weather condition (sunny or rainy), we can easily choose either the sunny model or the rainy model correspondingly.

C. Performance analysis

In this subsection, the accuracy and complexity of the proposed MLP-based channel model predicting/modeling channel attenuation 1 min–60 min in advance are shown.

1) Prediction accuracy: The accuracy of MLP-based channel model predicting channel attenuation 1 min–60 min in advance is measured via MSE between predicted and measured channel attenuation and the cumulative density function (CDF) of absolute error. The MSE reflects overall value of error while the CDF of absolute error shows the distribution of absolute errors.

The MSE between measured and predicted channel attenuation by using MLP-based channel model is shown in Table V in Appendix A. In this table, it can be seen that the MSE increases with the prediction window. For instance, the MSE of the general prediction with 60 min in advance by using the general model is approximately 0.43 dB larger than that of general prediction with 0 min in advance by using the general model. Similarly, the MSE of the sunny prediction with 60 min in advance by using the sunny model is approximately 0.44 dB larger than that of the sunny prediction with 0 min in advance by using the sunny model. However, the rainy prediction behaves differently from them. The MSEs of rainy prediction by using the general model and rainy model always fluctuate around 3-4 dB, whether the prediction time is 0 min or 60 min. The MSEs of rainy prediction by using the sunny model always fluctuate around 6 dB.

The CDFs of absolute error of general predictions with 0 min–60 min in advance by using the general model based on MLP are shown in Fig. 3. Predictions with 0 min, 5 min,

This article has been accepted for publication in a future issue of this journal, but has not been fully edited. Content may change prior to final publication. Citation information: DOI 10.1109/TVT.2020.3037212, IEEE Transactions on Vehicular Technology

and 45 min in advance have better performance when absolute error is below 0.4 dB. When absolute error is above 0.4 dB, the predictions with different minutes in advance have similar performance and increase slowly. Finally, more than 88% of the absolute errors between the predicted and measured channel attenuation are below 1 dB.

The comparison among prediction performances of general prediction, sunny prediction, and rainy prediction by using the general model, sunny model, and rainy model based on MLP is as follows. According to the comparison of MSE between predicted and measured channel attenuation, the general prediction with 0 min-60 min in advance has the best prediction performance by using the general model, better performance by using the sunny model, and the worst performance by using the rainy model, i.e. the MSEs of the general prediction with 1 min in advance by using the general model, sunny model, and rainy model are 0.558, 0.858, and 1.870, respectively. The sunny prediction with 0 min-60 min in advance has similar prediction performance by using the general model and the sunny model, but better performance by using the sunny model, i.e. the MSEs of the sunny prediction with 1 min in advance by using the general model and sunny model are 0.274 and 0.258. Using the rainy model delivers inferior performance, i.e. the MSE of sunny prediction with 20 min in advance by rainy model is 2.470. The rainy prediction with 0 min-60 min in advance has the best performance by using the rainy model and the worst performance by using the sunny model. The MSE of the rainy prediction with 4 min in advance by using the sunny model is up to 7.388, which is the highest value in Table. V.

The CDFs of absolute errors of predicting channel attenuation 10 min in advance by using MLP-based channel models is shown in Fig. 4. Although the MSEs of the sunny prediction with 0 min-60 min in advance by using the general model and the sunny model based on MLP are very similar, the low absolute error distribution of the sunny prediction by using the sunny model is higher than that of the sunny prediction by using the general model when absolute error is approximately 0 dB-0.5 dB as shown in Fig. 4. The two models are gradually converging when the absolute error increases to values higher than 0.5 dB. When the absolute error is approximately 0 dB-1.1 dB, the low absolute error distribution of the rainy prediction by using the general model is higher than that of the rainy prediction by using the rainy model. However, the low absolute error distribution of the rainy prediction by using the rainy model increases and is higher than that of rainy prediction by using the general model when absolute error increases higher than 1.1 dB. Meanwhile, the low absolute error distribution of sunny prediction by using the sunny model and the general model is higher than that of general prediction by using the general model. Therefore, the advantage of sunny prediction by using the sunny model is more significant in the analysis of CDFs of absolute error than the analysis of MSE. In conclusion, it can be seen the weather classification during the process of the database construction has important significance in satellite channel model.

2) Model complexity: The complexity of MLP-based channel model predicting channel attenuation 1 min–60 min in advance is measured via training time, loading time, and test time. It is shown in Table. VI. The training time and loading time of channel model based on MLP and test time do not vary with prediction time. In general, the training time of the sunny model is longer than that of general model and rainy model based on MLP. However, the test times of the general prediction by using the general model, sunny model, and rainy model based on MLP are very similar. The same conclusion applies to training time and loading time.

In aforementioned results, the MLP has in total six layers. The number of parameters of each layer is shown in Table III. The parameters of the first fully connection layer is related to the input layer. It has 112 parameters when the input layer is a 7-dimensional vector. The second to the fifth fully connection layers are symmetrical. Both the second and fifth fully connection layers have 512 parameters, respectively.

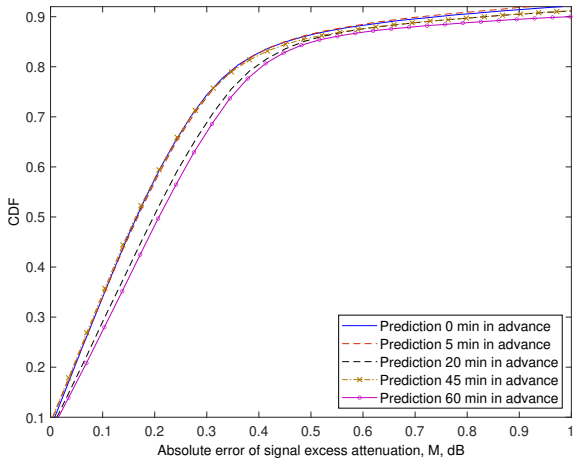

Fig. 3: The CDFs of absolute error of general prediction with 0 min–60 min in advance by using the general model based on MLP.

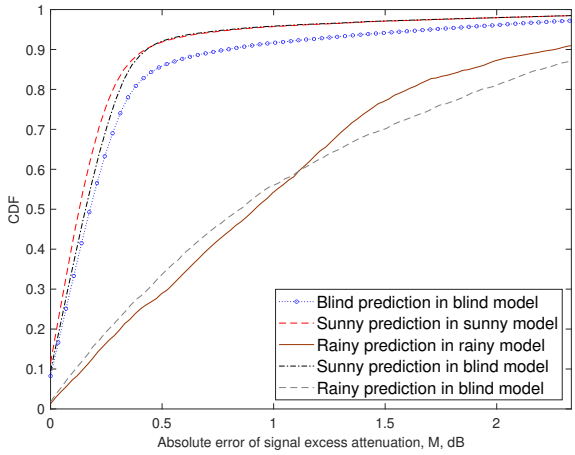

Fig. 4: The CDFs of absolute error of predicting channel attenuation 10 min in advance by using the MLP-based channel models.

This article has been accepted for publication in a future issue of this journal, but has not been fully edited. Content may change prior to final publication. Citation information: DOI 10.1109/TVT.2020.3037212, IEEE Transactions on Vehicular Technology

TABLE III: Number of parameters of MLP.

Layers	Number of parameters
Fully connection layer 1	112
Fully connection layer 2	512
Fully connection layer 3	2048
Fully connection layer 4	2048
Fully connection layer 5	512
Fully connection layer 6	16
Total	5248

Both the third and fourth fully connection layers have 2048 parameters which account for most parameters of the model. The final fully connection layer has 16 parameters. Then the number of total parameters of the model is 5248.

In summary, the conclusions of prediction accuracy and model complexity of channel model based on MLP are as follows.

1) Under the general prediction and sunny prediction, MSE between predicted and measured channel attenuation increases with the prediction window. However, the rainy prediction behaves differently. Its MSE always fluctuates, without monotonous change over time.
2) More than 88% of the absolute errors between the predicted and measured channel attenuation are less than 1 dB.
3) In the channel models based on MLP, the general prediction, sunny prediction, and rainy prediction are the best in the general model, sunny model, and rainy model, respectively. For instance, when we already know that it is raining, the MSE of rainy prediction is 4.73 and 3.21 with the general model and rainy model, respectively. This demonstrates the importance of weather classification.
4) According to the comparison of the training time, loading time, and test time, the complexity of the MLP-based model does not change drastically with the prediction time and weather classification.

IV. Channel Model Based on LSTM

A. System model

The recurrent neural network (RNN) with LSTM, proposed by S. Hochreiter and J. Schmidhuber in [35], can overcome the vanishing or exploding gradient problem. It is typically used in the learning problems related to sequential data to establish dependencies between states at long intervals. As the Fig. 5 shows, a LSTM block has three gates (input gate, forget gate, output gate), a block input, a memory cell, and a block output. A LSTM forward pass can be formalized as the follow

Block input:

$$\widetilde{c}_t = g(W_c \left[x_t + y_{t-1}\right] + b_c) \tag{5}$$

Input gate:

$$i_t = \sigma(W_i \left[x_t + y_{t-1}\right] + b_i) \tag{6}$$

Forget gate:

$$f_t = \sigma(W_f \left[x_t + y_{t-1}\right] + b_f) \tag{7}$$

Cell:

$$c_t = f_t \odot c_{t-1} + i_t \odot \widetilde{c}_t \tag{8}$$

Output gate:

$$o_t = \sigma(W_o \left[x_t + y_{t-1}\right] + b_o) \tag{9}$$

Block output:

$$y_t = o_t \odot h(c_t) \tag{10}$$

where W_c, W_i, W_f, W_o and b_c, b_i, b_f, b_o are respectively the weight matrix and the vector of bias in each gate; x_t and y_{t-1} are the input data at time t and the output vectors of the upper cell respectively. In the above equations, $\widetilde{c}_t$ is the extraction of the features of the current input for calculating the current memory cell c_t. It represents the output of the input gate which controls how many the information retains from upper cell to current memory cell c_t depend on current input. The variable f_t represents the output of the forget gate which decides the volume of information forgotten from the upper cell to the current memory depending on the current input. o_t is the output of the output gate which controls the volume of information retained from upper cell to output y_t of this cell. c_{t-1} is the retained information of the upper cell (upper memory). C_t represents the current memory of this cell which contains the information at long intervals. y_t is the output of this cell. σ, g, h is the activation function where σ is always the sigmoid function and g, h is usually the tanh function.

The detail model we designed is shown in Fig. 6. Four fully connected layers and 1 LSTM layer are applied. The input layer is a vector of 7-dimension or 14-dimension of atmosphere data. The output of LSTM layer is set to a 32-dimension vector. There are 16, 32, 64, 1 neurons for each fully connected layer. The loss function is MSE. Back propagation are applied end-to-end to optimize the weights of the model where is the RMSProp in [36] with momentum of 0.9 and smooth factor of 10^{-6}. The timestep is set different to find the best performance. Keras is used to build this model. The learning rate is set to 10^{-4}. 1000 epochs training times are set with early stop that has patience. The patience is set as 5. The initialization of each layer use the Xavier uniform initializer [37].

B. Weather classification and database description

For the comparison between the proposed channel model based on MLP and LSTM, the consistence of databases and datasets for training and testing the models should be kept. Therefore, in this subsection, we follow the same way to do the weather classification as well as the same definition given in Subsection III B. This means that the same entire database, sunny database, and rainy database are used to train and get the general model, sunny model, and rainy model, respectively. The definitions of the general prediction, sunny prediction, and rainy prediction are the same as those given in Subsection III B.

This article has been accepted for publication in a future issue of this journal, but has not been fully edited. Content may change prior to final publication. Citation information: DOI 10.1109/TVT.2020.3037212, IEEE Transactions on Vehicular Technology

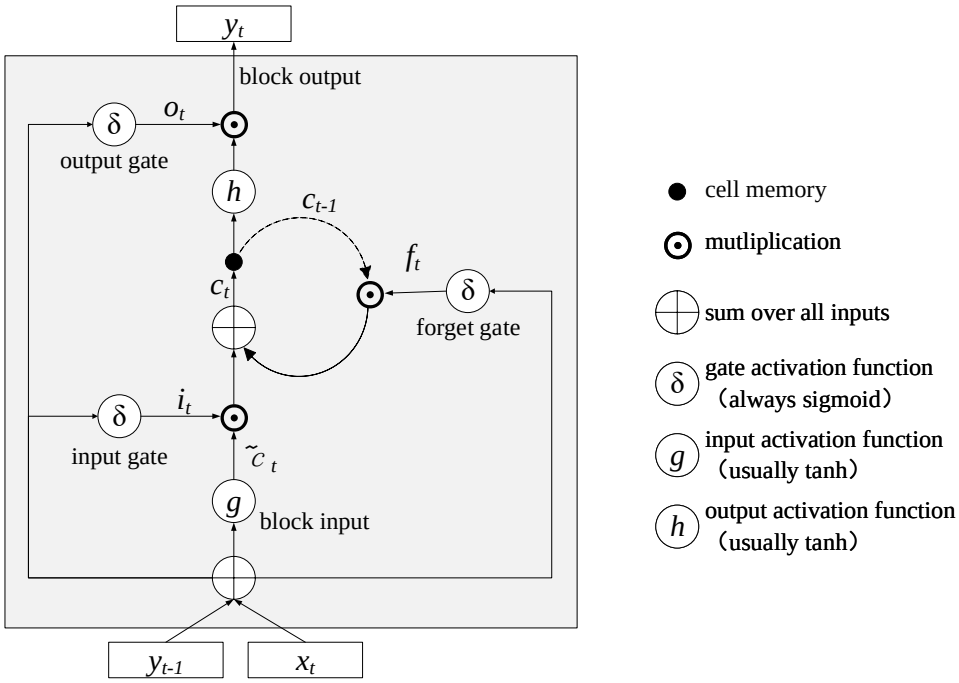

Fig. 5: A LSTM block.

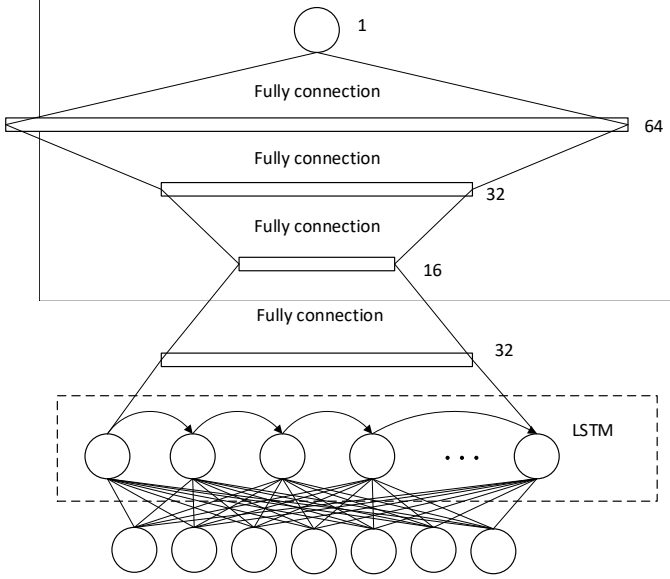

Fig. 6: The Structure of model we designed.

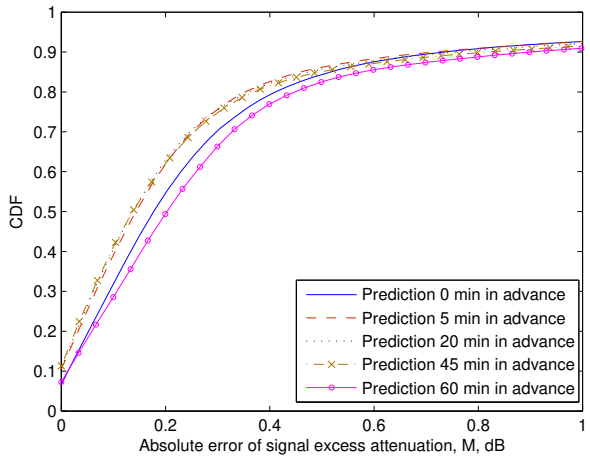

Fig. 7: The CDFs of absolute error of general prediction with 0 min–60 min in advance by using the general model based on LSTM.

C. Performance analysis

In this subsection, the accuracy and complexity of proposed LSTM-based channel model modeling/predicting channel attenuation 1 min–60 min in advance are shown.

1) Prediction accuracy: The accuracy of LSTM-based channel model with time step θ=0, 5, 10, and 15 min predicting channel attenuation 0 min–60 min in advance is measured via CDF of absolute error and MSE between predicted and measured channel attenuation.

As Table VII shows, the MSE between predicted and measured channel attenuation increases with prediction time, irrespective of whether the prediction time is 0 min or 60 min, as well as whether θ takes the value of 0 min or 15 min. For example, when θ=0 min, the MSE of the general prediction with 60 min in advance by using the general model based on LSTM is approximately larger 0.26 dB than that of the general prediction with 0 min in advance. Similarly, the MSE of the sunny prediction with 60 min in advance by using the sunny model is approximately larger 0.43 dB than that of the sunny prediction with 0 min in advance. However the rainy prediction by using the general model, sunny model and rainy model diverge. The MSEs of rainy prediction by using the general model and rainy model always fluctuate around 3 dB,

This article has been accepted for publication in a future issue of this journal, but has not been fully edited. Content may change prior to final publication. Citation information: DOI 10.1109/TVT.2020.3037212, IEEE Transactions on Vehicular Technology

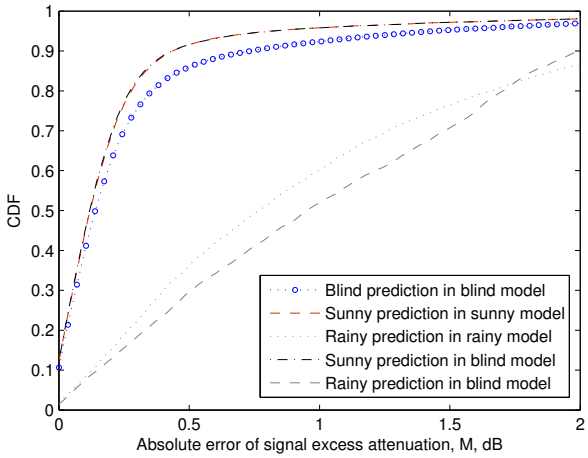

Fig. 8: The CDFs of absolute error of predicting channel attenuation 10 min in advance by the LSTM-based channel models.

without monotonous change over time. The MSEs of the rainy prediction by using the sunny model always fluctuate around 4 dB.

The CDF of absolute error of the general prediction with 0 min–60 min in advance by using the general model based on LSTM is shown in Fig. 7. When absolute error is below 0.5 dB, the cumulative distribution of absolute error of the general prediction with 5 min, 20 min, and 45 min in advance by using the general model increase faster. Especially, their cumulative distribution of absolute error below 0.2 dB has 5 % higher proportion than that of the general prediction with 0 min in advance by using the general model. This suggests prediction with 5 min, 20 min, and 45 min in advance have better performance when absolute error is below 0.5 dB. When absolute error is approximately above 0.8 dB, the prediction with 0 min, 5 min, 20 min, 45 min, and 60 min in advance have similar performance and increase slowly. As Fig. 7 shows, more than 90% of the absolute errors between the predicted and measured channel attenuation are less than 1 dB.

For researching the effectiveness of weather classification in LSTM-based channel model, the performance of the general prediction, sunny prediction, and rainy prediction by using the general model, sunny model, and rainy model based on LSTM is calculated and analyzed as follows.

According to the comparison of MSE between predicted and measured channel attenuation, the general prediction with 0 min-60 min in advance has the best prediction performance by using the general model, better performance by using the sunny model, and the worst performance by using the rainy model, i.e. the MSEs of the general prediction with 4 min in advance by using the general model, sunny model, and rainy model are 0.516, 0.843, and 2.700, respectively. The sunny prediction with 0 min-60 min in advance has very similar prediction performance by using the general model and sunny model, but better performance by using the sunny model, i.e. the MSEs of the sunny prediction with 45 min in advance by using the general model and sunny model are 0.780 and 0.816, respectively. It has inferior performance when using the rainy model based on LSTM. The rainy prediction with 0 min-60 min in advance has the best prediction performance by using the rainy model, better performance by using the general model, and the worst performance by using the sunny model. The MSE of the rainy prediction with 2 min in advance by the sunny model is up to 6.280, which is the highest value in Table VII.

The CDFs of absolute error of predicting channel attenuation 10 min in advance by using LSTM-based channel models is shown in Fig. 8. The cumulative distributions of absolute error of the sunny prediction by using the sunny model and general model are on a basic agreement. Combined with their MSE between predicted and measured channel attenuation, these results are summarised in Table VII. These results indicate that the accuracy of the sunny prediction by using the sunny model and the general model based on LSTM are in par. When absolute error is approximately 0 dB-1.6 dB, the low absolute error distribution of the rainy prediction by using the rainy model is higher than that of the rainy prediction by general model. Meanwhile, the low absolute error distribution of the sunny prediction by using the sunny model and general model is higher than that of the general prediction by using the general model. Combined with their MSEs between predicted and measured channel attenuation shown in Table VII, the advantage of the sunny prediction by using the sunny model is more obvious in the analysis of CDFs of absolute error than the analysis of MSE. In conclusion, it can be seen the weather classification is critical for the LSTM-based channel model.

2) Model complexity: The complexity of LSTM-based channel model predicting channel attenuation 0 min–60 min in advance is measured via training time, loading time, and test time.

This is shown in Table VIII. The training time and loading time of channel model and test time do not vary with prediction time. In general, the training time of the sunny model is longer than that of the general model and the rainy model. However, the test times of the general prediction by using the general model, the sunny model, and the rainy model are very similar. The same conclusion applies to the training time and loading time. It's worth noting that training time, loading time, and test time in Table VIII show 0 if it is very very small.

The LSTM has in total five layers (1 LSTM layer and 4 fully connection layers). The number of parameters of each layer is shown in Table IV. Most of the parameters are in the LSTM layer, accounting for more than 60 % of the model. The parameters of the LSTM layer are related to the input layer. There are 5120 parameters when then input layer is a 7-dimension vector. The first to the fourth fully connection layers have 512, 512, 2048, and 64 parameters, respectively. Then the number of total parameters of the model is 8256 parameters when the input layer is a 7-dimensional vector. Compared to the MLP, the deep of the model is more shallow, but the parameters of the model are larger.

3) Analysis of time step: Fig. 9 shows the comparison among MSEs of predicting channel attenuation 0 min-60 min in advance by LSTM-based channel models with different θ. In general, the prediction accuracy of LSTM-based channel

This article has been accepted for publication in a future issue of this journal, but has not been fully edited. Content may change prior to final publication. Citation information: DOI 10.1109/TVT.2020.3037212, IEEE Transactions on Vehicular Technology

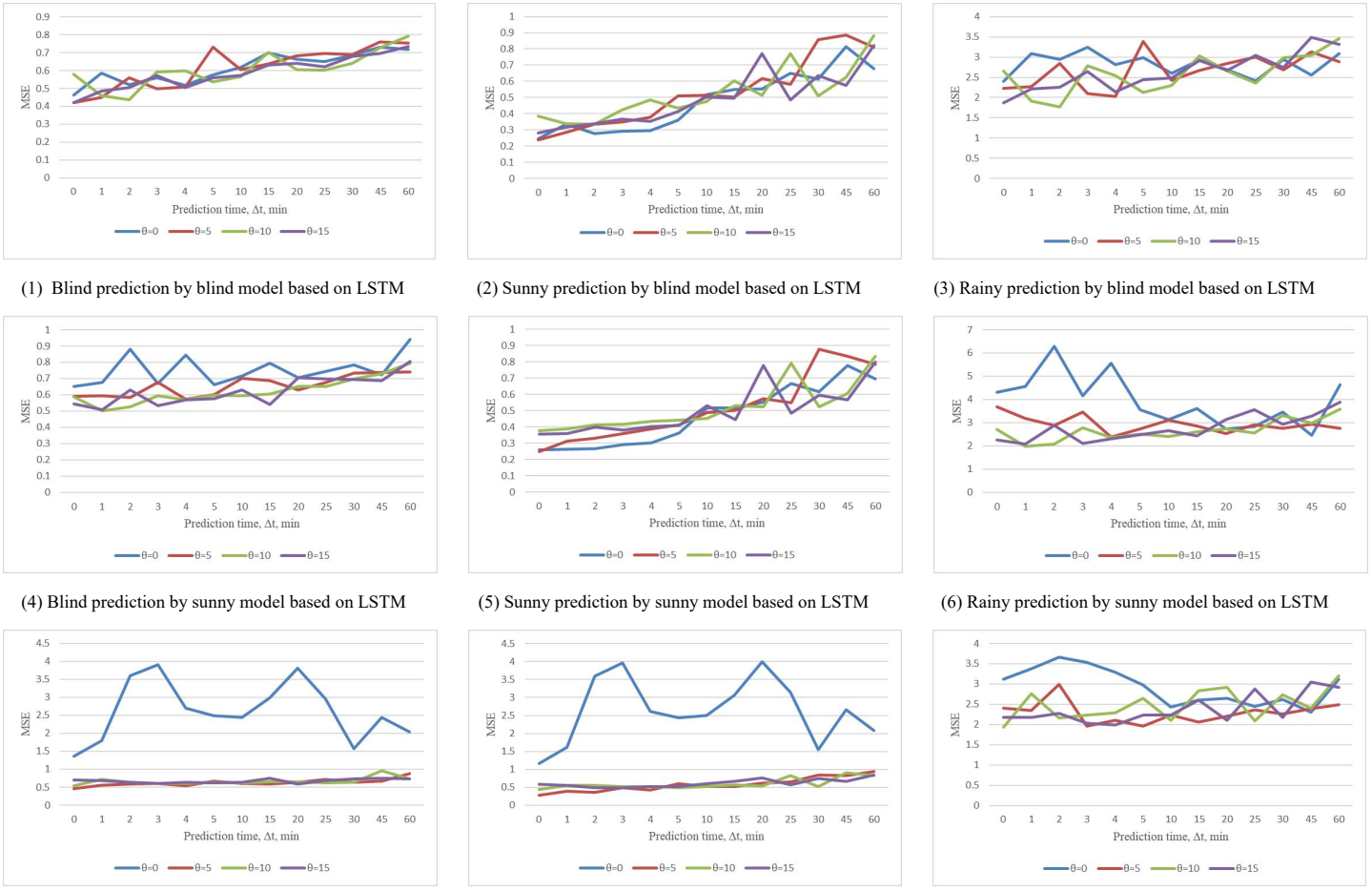

(1) Blind prediction by blind model based on LSTM

(2) Sunny prediction by blind model based on LSTM

(3) Rainy prediction by blind model based on LSTM

(4) Blind prediction by sunny model based on LSTM

(5) Sunny prediction by sunny model based on LSTM

(6) Rainy prediction by sunny model based on LSTM

(7) Blind prediction by rainy model based on LSTM

(8) Sunny prediction by rainy model based on LSTM

(9) Rainy prediction by rainy model based on LSTM

Fig. 9: The comparison of predicting channel attenuation 0 min-60 min in advance by the LSTM-based channel models with different θ.

TABLE IV: Number of parameters of LSTM.

Layers	Number of parameters
LSTM layer	5120
Fully connection layer 1	512
Fully connection layer 2	512
Fully connection layer 3	2048
Fully connection layer 4	64
Total	8256

model with θ=15 min is better and more stable as the purple line in Fig. 9 shows.

As Table VIII shown, the rank of training times of LSTM-based channel model with different θ is $\theta = 15 > \theta = 10 > \theta = 5 > \theta = 0$. Meanwhile, the rank of test times of LSTM-based channel model with different θ is also $\theta = 15 > \theta = 10 > \theta = 5 > \theta = 0$. So, the bigger θ, the higher the accuracy, and the model more complex.

In summary, the conclusions of prediction accuracy and model complexity of channel model based on LSTM are as follows.

1) Under the general prediction and sunny prediction, MSE between predicted and measured channel attenuation increases with the prediction window. However, the rainy prediction behaves differently. Its MSE always fluctuates, instead of steadily increasing with the prediction window.
2) More than 90% of the absolute errors between predicted and measured channel attenuation are less than 1 dB.
3) According to the CDF of absolute error and MSE analysis, the weather classification is critical for the channel models based on LSTM. The general prediction, sunny prediction, and rainy prediction are the best with the general model, sunny model, and rainy model, respectively.
4) Summarizing, the bigger the time step of LSTM, the higher the accuracy, and the model more complex. However, the influence of the time step is smaller in comparison with the weather classification.

V. Comparison of Channel Models based on MLP and LSTM with Weather Classification

Fig. 10 depicts the comparison between MSEs of channel models based on MLP and LSTM predicting channel attenuation 0 min-60 min in advance. As shows, only in the sunny

This article has been accepted for publication in a future issue of this journal, but has not been fully edited. Content may change prior to final publication. Citation information: DOI 10.1109/TVT.2020.3037212, IEEE Transactions on Vehicular Technology

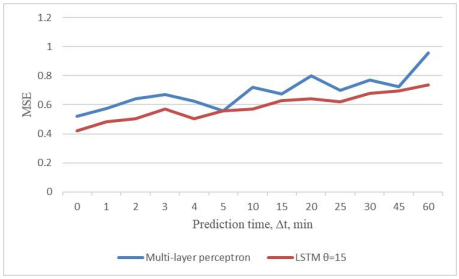

(1) Blind prediction by blind model based on LSTM

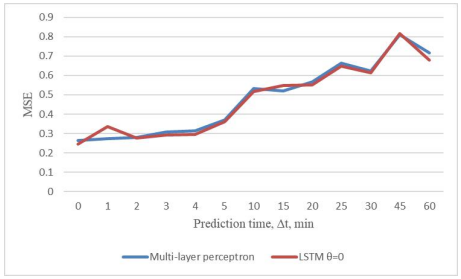

(2) Sunny prediction by blind model based on LSTM

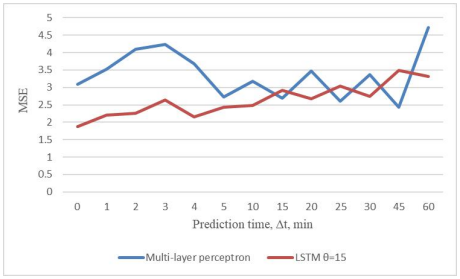

(3) Rainy prediction by blind model based on LSTM

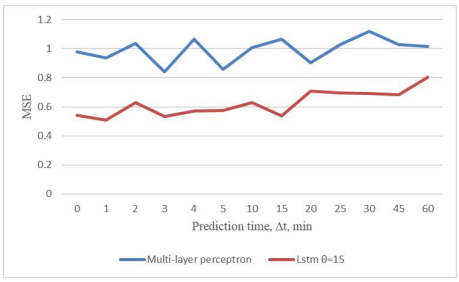

(4) Blind prediction by sunny model based on LSTM

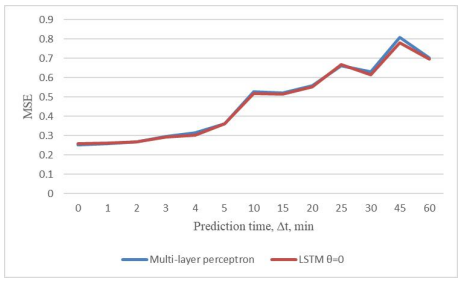

(5) Sunny prediction by sunny model based on LSTM

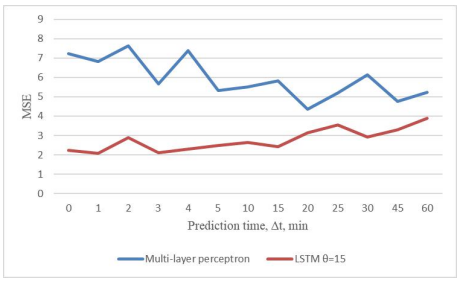

(6) Rainy prediction by sunny model based on LSTM

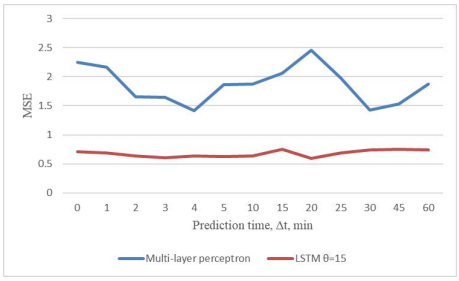

(7) Blind prediction by rainy model based on LSTM

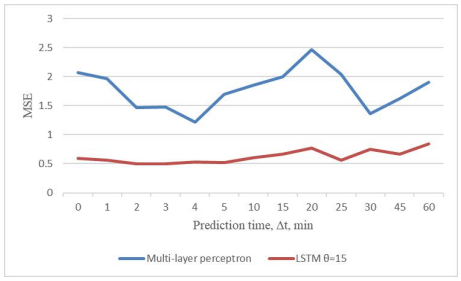

(8) Sunny prediction by rainy model based on LSTM

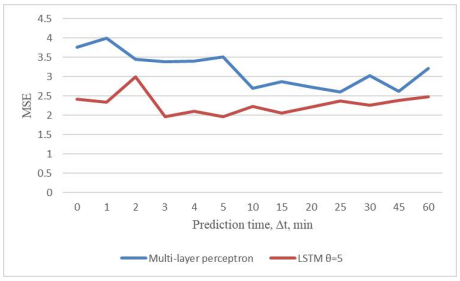

(9) Rainy prediction by rainy model based on LSTM

Fig. 10: The comparison between channel models based on MLP and LSTM predicting channel attenuation 0 min-60 min in advance.

prediction by using the general model and sunny model, the LSTM-based channel model has the similar accuracy performance with the MLP-based channel model. The accuracy of the LSTM-based channel model is better than that of the MLP-based channel model in other situations. The atmosphere data which affects the satellite channel attenuation significantly is in the form of time series, i.e. it is associated with time correlation. It has time correlation. Because of the memory feature of LSTM, the LSTM has its advantages in learning time series data. Therefore, the LSTM-based model has better performance on the satellite attenuation prediction than the MLP-based model. As Table VI and VII show, the test time of the LSTM-based channel model is more than that of the MLP-based channel model for the same prediction. In general, the LSTM-based channel model is more accurate and more complex than the MLP-based channel model.

Fig. 11 compares the MSE of the general prediction, sunny prediction, and rainy prediction by using channel models based on MLP and LSTM predicting channel attenuation 0 min-60 min in advance. When the weather condition is unknown, the general model based on LSTM has the best prediction performance. For the sunny prediction, the accuracy of the general models based on MLP and LSTM and the sunny models based on MLP and LSTM are similar, and they are better than these of the rainy models based on MLP and LSTM. For the rainy prediction, the accuracy of the general models based on MLP and LSTM and the rainy models based on MLP and LSTM are very similar, but they are better than these of sunny model based on MLP and LSTM. Meanwhile, the accuracy of the general model and rainy model based on LSTM are better than these of the general model and rainy model based on MLP. With prediction time increases, the accuracy of the rainy model based on LSTM is better than that of the general model based on LSTM.

In summary, considering both the accuracy and complexity, the best tool for general prediction, sunny prediction, and rainy prediction are respectively: the general model based on LSTM, the sunny model based on MLP, and the rainy model based on LSTM.

VI. Conclusions

In this paper, we have proposed an atmosphere-informed data-driven predictive satellite channel model at Q-band based on MLP and LSTM to model/predict channel attenuation at

This article has been accepted for publication in a future issue of this journal, but has not been fully edited. Content may change prior to final publication. Citation information: DOI 10.1109/TVT.2020.3037212, IEEE Transactions on Vehicular Technology

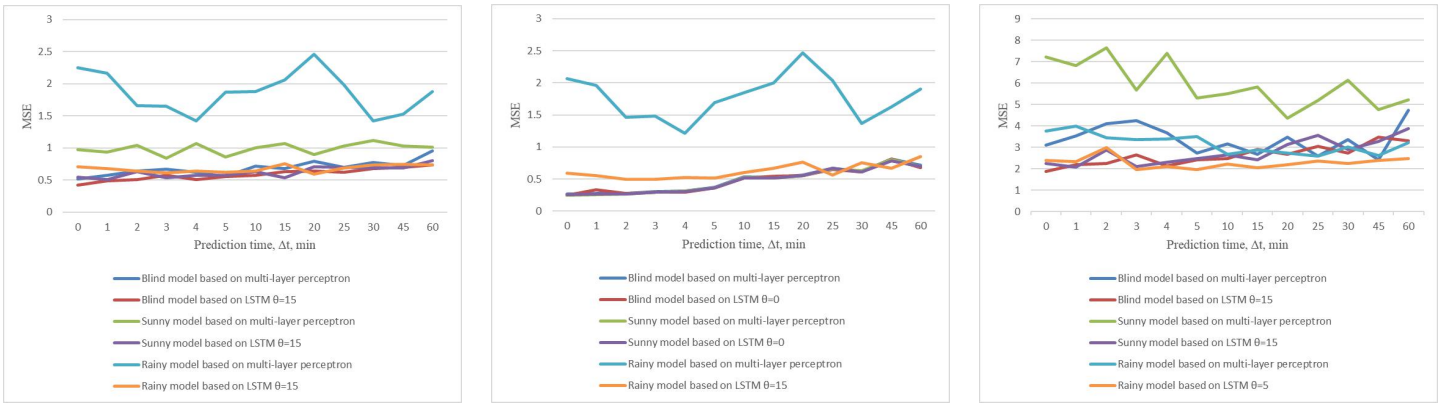

(1) Blind prediction (2) Sunny prediction (3) Rainy prediction

Fig. 11: The comparison among the general prediction, sunny prediction, and rainy prediction by using the channel models based on MLP and LSTM predicting channel attenuation 0 min-60 min in advance.

any interesting and specific time. Based on atmosphere data at a certain time, the proposed channel model can not only model the channel attenuation at this certain time, but also predict the channel attenuation of any specific time afterward. The propagation measurement by Alphasat beacon receiver and corresponding atmosphere measurement have been carried out at Chilbolton, Hampshire, UK. Based on the established measurement campaign, the accuracy and complexity of the proposed channel model has been investigated and analyzed in detail. Statistical analysis demonstrated that the weather classification can further improve the accuracy of the proposed channel model. Compared with the MLP-based model, the LSTM-based model has a significant advantage in modeling/predicting satellite channel attenuation. However, the performance of LSTM-based model increases slightly with the time step window. Considering both the accuracy and complexity, the optimal option is that the sunny model based on MLP and the rainy model based on LSTM are preferred for sunny prediction and rainy prediction with simple inspection of weather conditions as a prior information. Moreover, the utility of the proposed model has been validated by the close agreement between the attenuation modeled/predicted by the proposed model and the one from real measured data. These interesting observations and useful conclusions are important and useful for the better design of B5G/6G satellite-terrestrial wireless communication systems.

APPENDIX A
THE MSE AND COMPLEXITY OF THE MLP-BASED CHANNEL MODEL

Tables V and Tables VI list the MSE and complexity of the MLP-based channel model in this paper.

APPENDIX B
THE MSE AND COMPLEXITY OF THE LSTM-BASED CHANNEL MODEL

Table VII and Table VIII list the MSE and complexity of the LSTM-based channel model in this paper.

REFERENCES

[1] Ericsson, "Ericsson mobility report," 4th Quater, 2019. [Online] Available: https://www.ericsson.com/491b06/assets/local/mobility-report/documents/2019/ericsson-mobility-report-q4-2019-update.pdf.

[2] Facebook, "With more than half the world online, how do we connect the rest?", Feb. 2020. [Online] Available: https://about.fb.com/news/2020/02/inclusive-internet-index/.

[3] Z. Huang and X. Cheng, "A general 3D space-time-frequency non-stationary model for 6G channels," *IEEE Trans. Wireless Commun.*, accepted.

[4] W. J. Vogel and G. W. Torrence, "Propagation measurements for satellite radio reception inside buildings," *IEEE Trans. Antennas Propaga.*, vol. 41, no. 7, pp. 954–961, Jul. 1993.

[5] M. Cheffena and F. Perez-Fontan, "Land mobile satellite channel simulator along roadside trees," *IEEE Trans. Antennas Propag.*, vol. 9, pp. 748–751, 2010.

[6] W. J. Vogel and N. Kleiner, "Propagation measurements for satellite services into buildings," in *Proc. IEEE Aerospace Conference*, Snowmass, Aspen, CO, 1997, pp. 91–107.

[7] E. Cid, M. G. Sanchez, and A. V. Alejos, "Wideband analysis of the satellite communication channel at Ku- and X-bands," *IEEE Trans. Veh. Technol.*, vol. 65, no. 4, pp. 2787–2790, Apr. 2016.

[8] C. Kourogiorgas, P. Arapoglou, and A. Panagopoulos, "Statistical Characterization of adjacent satellite interference for earth stations on mobile platforms operating at Ku and Ka-bands," *IEEE Wireless Commun. Lett.* , vol. 4, no. 1, pp. 82–85, Feb. 2015.

[9] W. J. Vogel and J. Goldhirsh, "Earth-satellite tree attenuation at 20 GHz: foliage effects," *Electronics Letters*, vol. 29, no. 18, pp. 1640–1641, Sept. 1993.

[10] S. Gong, K. Xie, X. Li, J. Huang, L. Zhang, and H. Shi, "Modifying the parameters of specific attenuation model for prediction attenuation induced by rain at Ka-band in Xi'an, China," in *Proc. International Symposium on Antennas, Propagation and EM Theory*, Guangzhou, 2010, pp. 606–609.

[11] J. Huang, S. Gong, and B. Cai, "The frequency scaling ratio factor of rain attenuation in Ka-waveband along earth-space path in China," in *Proc. International Conference on Mechanic Automation and Control Engineering*, Hohhot, 2011, pp. 7831–7833.

[12] S. Gong, D. Wei, X. Xue, and M. Y. Chen, "Study on the channel model and BER performance of single-polarization satellite-earth MIMO communication systems at Ka-band," *IEEE Trans. Antennas Propaga.*, vol. 62, no. 10, pp. 5282–5297, Oct. 2014.

[13] M. D. Sanctis, T. Rossi, and M. Ruggieri et al., "Performance evaluation of fading estimation techniques over Q/V band satellite links," in *Proc. IEEE Aerospace Conference'18*, Big Sky, MT, USA, 2018, pp. 1-6.

[14] A. Costouri, J. Nessel, and G. Goussetis, "Validation of a digital noise power integration technique for radiometric clear sky attenuation estimation at Q-band," *IEEE Antennas and Propagation*, vol. 68, no. 9, pp. 6743–6751, Sept. 2020.

This article has been accepted for publication in a future issue of this journal, but has not been fully edited. Content may change prior to final publication. Citation information: DOI 10.1109/TVT.2020.3037212, IEEE Transactions on Vehicular Technology

TABLE V: The MSE of the MLP-based channel model.

Model	MSE	0	1	2	3	4	5	10	15	20	25	30	45	60
Blind Model	Train Set	6.15E-01	6.92E-01	7.58E-01	8.76E-01	7.55E-01	7.76E-01	8.35E-01	9.11E-01	9.11E-01	9.06E-01	9.23E-01	9.41E-01	1.04E+00
	Validation Set	9.06E-01	1.03E+00	1.17E+00	1.19E+00	1.15E+00	1.02E+00	1.28E+00	1.28E+00	1.40E+00	1.33E+00	1.44E+00	1.42E+00	1.59E+00
	Blind Prediction	5.22E-01	5.75E-01	6.42E-01	6.69E-01	6.24E-01	5.58E-01	7.21E-01	6.76E-01	7.98E-01	7.01E-01	7.72E-01	7.24E-01	9.58E-01
	Sunny Prediction	2.64E-01	2.74E-01	2.80E-01	3.08E-01	3.16E-01	3.70E-01	5.33E-01	5.22E-01	5.66E-01	6.65E-01	6.22E-01	8.09E-01	7.18E-01
	Rainy Prediction	3.10E+00	3.53E+00	4.10E+00	4.24E+00	3.69E+00	2.73E+00	3.17E+00	2.69E+00	3.47E+00	2.60E+00	3.37E+00	2.43E+00	4.73E+00
Sunny Model	Train Set	2.26E-01	2.29E-01	2.36E-01	2.34E-01	2.51E-01	2.62E-01	3.27E-01	3.61E-01	3.83E-01	4.13E-01	4.64E-01	5.04E-01	5.40E-01
	Validation Set	1.94E-01	1.95E-01	2.28E-01	2.35E-01	2.24E-01	2.21E-01	2.54E-01	2.75E-01	3.14E-01	4.15E-01	5.17E-01	7.81E-01	7.37E-01
	Blind Prediction	9.77E-01	9.36E-01	1.04E+00	8.41E-01	1.07E+00	8.58E-01	1.01E+00	1.07E+00	9.03E-01	1.03E+00	1.12E+00	1.03E+00	1.02E+00
	Sunny Prediction	2.52E-01	2.58E-01	2.70E-01	2.96E-01	3.16E-01	3.61E-01	5.27E-01	5.20E-01	5.58E-01	6.62E-01	6.30E-01	8.07E-01	7.01E-01
	Rainy Prediction	7.23E+00	6.82E+00	7.65E+00	5.68E+00	7.39E+00	5.31E+00	5.50E+00	5.83E+00	4.36E+00	5.20E+00	6.14E+00	4.76E+00	5.23E+00
Rainy Model	Train Set	6.62E+00	7.26E+00	7.39E+00	7.06E+00	7.59E+00	7.50E+00	7.45E+00	7.71E+00	7.96E+00	7.70E+00	7.03E+00	6.34E+00	6.31E+00
	Validation Set	7.40E+00	7.74E+00	6.65E+00	6.82E+00	7.22E+00	8.79E+00	7.37E+00	8.70E+00	8.92E+00	7.89E+00	7.80E+00	7.09E+00	7.38E+00
	Blind Prediction	2.25E+00	2.16E+00	1.66E+00	1.65E+00	1.42E+00	1.87E+00	1.88E+00	2.06E+00	2.46E+00	1.98E+00	1.42E+00	1.53E+00	1.87E+00
	Sunny Prediction	2.07E+00	1.96E+00	1.47E+00	1.48E+00	1.21E+00	1.69E+00	1.85E+00	2.00E+00	2.47E+00	2.04E+00	1.36E+00	1.63E+00	1.90E+00
	Rainy Prediction	3.76E+00	3.99E+00	3.45E+00	3.38E+00	3.40E+00	3.52E+00	2.69E+00	2.87E+00	2.73E+00	2.60E+00	3.02E+00	2.62E+00	3.21E+00

TABLE VI: The complexity of the MLP-based channel model.

Model	Time (s)	0	1	2	3	4	5	10	15	20	25	30	45	60
Blind Model	Training Time	2.88E+01	1.89E+01	3.24E+01	1.00E+01	1.95E+01	1.97E+01	1.87E+01	1.28E+01	1.41E+01	1.97E+01	2.19E+01	1.98E+01	1.00E+01
	Loading Time	5.98E-03	6.01E-03	9.97E-03	9.00E-03	1.00E-02	9.00E-03	9.00E-03	1.00E-02	1.00E-02	1.00E-02	9.01E-03	9.01E-03	9.01E-03
	Blind Prediction	1.87E-01	1.62E-01	1.64E-01	1.61E-01	1.73E-01	1.71E-01	1.67E-01	1.65E-01	1.71E-01	1.66E-01	1.67E-01	1.72E-01	1.66E-01
	Sunny Prediction	1.35E-01	1.31E-01	1.32E-01	1.31E-01	1.29E-01	1.30E-01	1.37E-01	1.33E-01	1.39E-01	1.31E-01	1.33E-01	1.36E-01	1.28E-01
	Rainy Prediction	3.29E-02	2.89E-02	3.19E-02	2.99E-02	3.00E-02	3.29E-02	2.99E-02	2.99E-02	2.99E-02	2.99E-02	2.99E-02	2.99E-02	2.99E-02
Sunny Model	Training Time	4.72E+01	3.00E+01	2.08E+01	3.78E+01	1.55E+01	4.53E+01	2.60E+01	2.00E+01	2.07E+01	1.65E+01	9.25E+00	4.04E+01	2.04E+01
	Loading Time	1.00E-02	8.97E-03	8.98E-03	1.00E-02	9.00E-03	9.00E-03	1.00E-02	1.00E-02	1.00E-02	1.00E-02	9.97E-03	9.97E-03	8.98E-03
	Blind Prediction	1.67E-01	1.63E-01	1.67E-01	1.70E-01	1.59E-01	1.70E-01	1.70E-01	1.70E-01	1.65E-01	1.68E-01	1.68E-01	1.67E-01	1.69E-01
	Sunny Prediction	1.26E-01	1.32E-01	1.39E-01	1.31E-01	1.25E-01	1.35E-01	1.33E-01	1.41E-01	1.39E-01	1.32E-01	1.37E-01	1.35E-01	1.38E-01
	Rainy Prediction	2.99E-02	2.89E-02	3.00E-02	2.99E-02	2.90E-02	2.99E-02	2.99E-02	2.99E-02	2.99E-02	2.89E-02	2.99E-02	3.09E-02	2.99E-02
Rainy Model	Training Time	5.90E+00	4.86E+00	4.81E+00	4.79E+00	6.15E+00	6.21E+00	5.69E+00	5.31E+00	4.37E+00	3.43E+00	3.54E+00	2.85E+00	7.90E+00
	Loading Time	5.98E-03	9.97E-03	9.97E-03	9.97E-03	1.00E-02	1.00E-02	1.00E-02	9.00E-03	9.00E-03	8.90E-03	9.96E-03	8.98E-03	8.98E-03
	Blind Prediction	1.67E-01	1.71E-01	1.69E-01	1.68E-01	1.74E-01	1.64E-01	3.92E-01	1.69E-01	1.73E-01	1.67E-01	1.65E-01	1.67E-01	1.74E-01
	Sunny Prediction	1.35E-01	1.33E-01	1.35E-01	1.37E-01	1.33E-01	1.38E-01	1.38E-01	1.35E-01	1.30E-01	1.32E-01	1.30E-01	1.33E-01	1.36E-01
	Rainy Prediction	2.99E-02	2.89E-02	2.99E-02	2.99E-02	2.99E-02	2.90E-02	2.99E-02	2.99E-02	2.89E-02	2.99E-02	2.99E-02	2.90E-02	2.99E-02

TABLE VII: The MSE of the LSTM-based channel model.

	Prediction Time	0				1				2				3				4				5			
	Time Step	0	5	10	15	0	5	10	15	0	5	10	15	0	5	10	15	0	5	10	15	0	5	10	15
Blind Model	Train Set	5.10E-01	4.68E-01	5.00E-01	4.58E-01	5.12E-01	4.96E-01	4.93E-01	5.24E-01	7.23E-01	5.39E-01	5.27E-01	5.65E-01	5.70E-01	5.70E-01	5.59E-01	5.47E-01	5.89E-01	5.97E-01	7.05E-01	5.82E-01	6.09E-01	7.11E-01	6.37E-01	6.12E-01
	Validation Set	7.86E-01	7.16E-01	7.89E-01	7.25E-01	7.97E-01	7.78E-01	7.88E-01	7.80E-01	8.95E-01	8.68E-01	8.67E-01	8.17E-01	9.15E-01	8.96E-01	8.79E-01	8.58E-01	9.62E-01	9.82E-01	9.43E-01	8.81E-01	9.72E-01	1.03E+00	9.12E-01	9.26E-01
	Blind Prediction	4.64E-01	4.20E-01	5.81E-01	4.20E-01	5.84E-01	4.49E-01	4.59E-01	4.84E-01	5.21E-01	5.58E-01	4.36E-01	5.04E-01	5.60E-01	4.98E-01	5.93E-01	5.72E-01	5.16E-01	5.08E-01	5.98E-01	5.03E-01	5.75E-01	7.31E-01	5.36E-01	5.60E-01
	Sunny Prediction	2.44E-01	2.40E-01	3.85E-01	2.80E-01	3.36E-01	2.84E-01	3.38E-01	3.17E-01	2.77E-01	3.36E-01	3.35E-01	3.37E-01	2.92E-01	3.47E-01	4.24E-01	3.67E-01	2.95E-01	3.77E-01	4.85E-01	3.53E-01	3.61E-01	5.10E-01	4.35E-01	4.13E-01
	Rainy Prediction	2.40E+00	2.22E+00	2.66E+00	1.87E+00	3.08E+00	2.27E+00	1.91E+00	2.21E+00	2.94E+00	2.85E+00	1.77E+00	2.25E+00	3.25E+00	2.09E+00	2.78E+00	2.64E+00	2.82E+00	2.03E+00	2.54E+00	2.15E+00	2.98E+00	3.38E+00	2.13E+00	2.44E+00
Sunny Model	Train Set	2.22E-01	2.25E-01	2.71E-01	3.11E-01	2.22E-01	2.52E-01	2.95E-01	3.24E-01	2.34E-01	2.55E-01	2.92E-01	3.23E-01	2.28E-01	2.67E-01	2.96E-01	3.34E-01	2.48E-01	2.81E-01	3.26E-01	3.35E-01	2.57E-01	2.87E-01	3.17E-01	3.23E-01
	Validation Set	1.96E-01	2.00E-01	2.06E-01	2.16E-01	1.98E-01	2.04E-01	2.20E-01	2.13E-01	2.28E-01	2.19E-01	2.31E-01	2.28E-01	2.34E-01	2.15E-01	2.35E-01	2.25E-01	2.26E-01	2.16E-01	2.35E-01	2.37E-01	2.21E-01	2.20E-01	2.33E-01	2.47E-01
	Blind Prediction	6.53E-01	5.92E-01	5.87E-01	5.44E-01	6.76E-01	5.94E-01	5.01E-01	5.10E-01	8.80E-01	5.85E-01	5.26E-01	6.29E-01	6.69E-01	6.75E-01	5.93E-01	5.34E-01	8.43E-01	5.71E-01	5.69E-01	5.70E-01	6.62E-01	6.03E-01	5.96E-01	5.76E-01
	Sunny Prediction	2.60E-01	2.50E-01	3.77E-01	3.57E-01	2.63E-01	3.15E-01	3.88E-01	3.60E-01	2.68E-01	3.32E-01	4.14E-01	3.99E-01	2.92E-01	3.59E-01	4.18E-01	3.82E-01	3.03E-01	3.90E-01	4.35E-01	4.03E-01	3.62E-01	4.12E-01	4.41E-01	4.09E-01
	Rainy Prediction	4.30E+00	3.69E+00	2.70E+00	2.25E+00	4.56E+00	3.18E+00	1.97E+00	2.08E+00	6.28E+00	2.89E+00	2.08E+00	2.89E+00	4.16E+00	3.45E+00	2.78E+00	2.11E+00	5.57E+00	2.39E+00	2.35E+00	2.31E+00	3.55E+00	2.72E+00	2.49E+00	2.48E+00
Rainy Model	Train Set	8.22E+00	6.06E+00	5.53E+00	5.07E+00	8.46E+00	6.22E+00	5.32E+00	5.41E+00	8.71E+00	6.36E+00	5.74E+00	5.34E+00	8.74E+00	6.09E+00	5.54E+00	5.51E+00	8.45E+00	5.90E+00	5.47E+00	5.62E+00	8.36E+00	6.37E+00	5.90E+00	6.13E+00
	Validation Set	7.57E+00	5.49E+00	5.37E+00	5.41E+00	8.03E+00	6.33E+00	5.69E+00	5.87E+00	8.78E+00	6.57E+00	5.49E+00	5.54E+00	8.89E+00	5.85E+00	5.36E+00	5.82E+00	8.34E+00	5.80E+00	5.34E+00	5.65E+00	8.30E+00	5.99E+00	6.35E+00	6.03E+00
	Blind Prediction	1.36E+00	4.55E-01	5.39E-01	7.05E-01	1.80E+00	5.61E-01	7.11E-01	6.83E-01	3.59E+00	5.94E-01	6.33E-01	6.37E-01	3.91E+00	6.07E-01	6.08E-01	6.10E-01	2.70E+00	5.41E-01	6.10E-01	6.38E-01	2.49E+00	6.62E-01	6.30E-01	6.26E-01
	Sunny Prediction	1.16E+00	2.74E-01	4.40E-01	5.93E-01	1.62E+00	3.98E-01	5.59E-01	5.59E-01	3.59E+00	3.67E-01	5.49E-01	4.96E-01	3.96E+00	4.96E-01	5.27E-01	4.95E-01	2.61E+00	4.23E-01	5.19E-01	5.28E-01	2.44E+00	5.96E-01	4.87E-01	5.16E-01
	Rainy Prediction	3.12E+00	2.41E+00	1.93E+00	2.18E+00	3.38E+00	2.34E+00	2.76E+00	2.17E+00	3.67E+00	2.99E+00	2.17E+00	2.27E+00	3.53E+00	1.97E+00	2.23E+00	2.03E+00	3.29E+00	2.10E+00	2.30E+00	1.99E+00	2.97E+00	1.96E+00	2.64E+00	2.24E+00

	Prediction Time	10				15				20				25				30				45				60			
	Time Step	0	5	10	15	0	5	10	15	0	5	10	15	0	5	10	15	0	5	10	15	0	5	10	15	0	5	10	15
Blind Model	Train Set	7.06E-01	7.04E-01	6.97E-01	6.93E-01	7.39E-01	8.10E-01	7.42E-01	7.31E-01	7.83E-01	7.58E-01	7.65E-01	7.58E-01	8.96E-01	7.98E-01	7.80E-01	8.36E-01	8.32E-01	8.68E-01	8.20E-01	8.10E-01	8.60E-01	9.15E-01	8.39E-01	9.01E-01	9.81E-01	9.41E-01	9.32E-01	8.81E-01
	Validation Set	1.05E+00	1.05E+00	1.06E+00	1.04E+00	1.14E+00	1.24E+00	1.14E+00	1.13E+00	1.19E+00	1.20E+00	1.19E+00	1.21E+00	1.24E+00	1.29E+00	1.26E+00	1.29E+00	1.34E+00	1.35E+00	1.36E+00	1.33E+00	1.43E+00	1.45E+00	1.42E+00	1.39E+00	1.45E+00	1.44E+00	1.46E+00	1.43E+00
	Blind Prediction	6.19E-01	6.05E-01	5.68E-01	5.73E-01	6.99E-01	6.39E-01	7.01E-01	6.31E-01	6.65E-01	6.82E-01	6.05E-01	6.40E-01	6.52E-01	6.96E-01	6.03E-01	6.22E-01	6.88E-01	6.89E-01	6.40E-01	6.79E-01	7.30E-01	7.61E-01	7.27E-01	6.96E-01	7.20E-01	7.52E-01	7.93E-01	7.36E-01
	Sunny Prediction	5.17E-01	5.14E-01	4.74E-01	5.04E-01	5.49E-01	5.02E-01	6.04E-01	4.94E-01	5.53E-01	6.18E-01	5.12E-01	7.71E-01	6.49E-01	5.80E-01	7.72E-01	4.86E-01	6.15E-01	8.58E-01	5.09E-01	6.35E-01	8.16E-01	8.87E-01	6.26E-01	5.75E-01	6.78E-01	8.10E-01	8.84E-01	8.21E-01
	Rainy Prediction	2.60E+00	2.43E+00	2.30E+00	2.48E+00	2.94E+00	2.67E+00	3.03E+00	2.92E+00	2.69E+00	2.84E+00	2.65E+00	2.67E+00	2.41E+00	3.00E+00	2.36E+00	3.04E+00	2.95E+00	2.68E+00	2.98E+00	2.75E+00	2.56E+00	3.13E+00	3.04E+00	3.48E+00	3.08E+00	2.89E+00	3.46E+00	3.31E+00
Sunny Model	Train Set	3.19E-01	3.30E-01	3.44E-01	3.70E-01	3.54E-01	3.56E-01	3.64E-01	3.88E-01	3.76E-01	3.78E-01	4.32E-01	4.16E-01	4.04E-01	4.26E-01	4.33E-01	4.43E-01	4.49E-01	4.60E-01	4.74E-01	4.62E-01	4.97E-01	4.95E-01	5.03E-01	5.09E-01	5.37E-01	5.39E-01	5.55E-01	5.50E-01
	Validation Set	2.53E-01	2.54E-01	2.64E-01	3.25E-01	2.72E-01	2.79E-01	3.38E-01	4.10E-01	3.13E-01	3.64E-01	4.46E-01	4.95E-01	4.14E-01	4.71E-01	5.27E-01	6.49E-01	5.10E-01	5.65E-01	6.81E-01	7.02E-01	7.92E-01	7.56E-01	7.47E-01	7.12E-01	7.36E-01	7.30E-01	7.76E-01	7.87E-01
	Blind Prediction	7.17E-01	7.00E-01	5.96E-01	6.30E-01	7.95E-01	6.87E-01	6.05E-01	5.39E-01	7.03E-01	6.31E-01	6.51E-01	7.07E-01	7.46E-01	6.75E-01	6.51E-01	6.97E-01	7.82E-01	7.33E-01	6.99E-01	6.92E-01	7.24E-01	7.37E-01	7.30E-01	6.85E-01	9.41E-01	7.40E-01	7.96E-01	8.04E-01
	Sunny Prediction	5.17E-01	4.87E-01	4.53E-01	5.31E-01	5.16E-01	5.02E-01	5.31E-01	4.45E-01	5.53E-01	5.75E-01	5.24E-01	7.76E-01	6.67E-01	5.49E-01	7.94E-01	4.86E-01	6.16E-01	8.79E-01	5.23E-01	5.97E-01	7.80E-01	8.36E-01	6.06E-01	5.68E-01	6.95E-01	7.85E-01	8.34E-01	8.01E-01
	Rainy Prediction	3.12E+00	3.11E+00	2.42E+00	2.65E+00	3.60E+00	2.86E+00	2.60E+00	2.42E+00	2.74E+00	2.53E+00	2.74E+00	3.13E+00	2.84E+00	2.92E+00	2.56E+00	3.56E+00	3.47E+00	2.76E+00	3.30E+00	2.92E+00	2.44E+00	2.94E+00	2.98E+00	3.29E+00	4.64E+00	2.76E+00	3.58E+00	3.88E+00
Rainy Model	Train Set	8.03E+00	6.21E+00	5.94E+00	5.68E+00	7.93E+00	6.78E+00	6.00E+00	5.60E+00	7.93E+00	6.58E+00	5.82E+00	5.51E+00	7.55E+00	6.39E+00	5.71E+00	5.58E+00	6.90E+00	5.83E+00	5.67E+00	5.05E+00	6.16E+00	5.57E+00	6.01E+00	5.65E+00	6.26E+00	5.75E+00	5.02E+00	4.98E+00
	Validation Set	8.20E+00	6.15E+00	5.90E+00	5.40E+00	8.38E+00	6.34E+00	6.08E+00	6.24E+00	8.44E+00	5.85E+00	6.65E+00	4.26E+00	7.72E+00	6.73E+00	4.49E+00	6.89E+00	7.80E+00	4.67E+00	6.74E+00	6.25E+00	6.90E+00	4.78E+00	7.03E+00	6.43E+00	7.57E+00	6.15E+00	5.33E+00	5.05E+00
	Blind Prediction	2.44E+00	6.01E-01	6.13E-01	6.36E-01	2.98E+00	5.85E-01	6.60E-01	7.55E-01	3.81E+00	6.34E-01	6.57E-01	5.93E-01	2.96E+00	7.10E-01	6.26E-01	6.87E-01	1.57E+00	6.36E-01	6.38E-01	7.37E-01	2.44E+00	6.68E-01	9.54E-01	7.46E-01	2.03E+00	8.86E-01	7.40E-01	7.38E-01
	Sunny Prediction	2.49E+00	5.22E-01	5.28E-01	6.00E-01	3.06E+00	5.14E-01	5.73E-01	6.71E-01	3.99E+00	6.22E-01	5.34E-01	7.67E-01	3.14E+00	6.42E-01	8.28E-01	5.65E-01	1.56E+00	8.43E-01	5.28E-01	7.53E-01	2.66E+00	8.25E-01	9.08E-01	6.65E-01	2.08E+00	9.47E-01	8.28E-01	8.48E-01
	Rainy Prediction	2.44E+00	2.23E+00	2.10E+00	2.23E+00	2.61E+00	2.06E+00	2.83E+00	2.61E+00	2.65E+00	2.21E+00	2.92E+00	2.11E+00	2.45E+00	2.37E+00	2.09E+00	2.88E+00	2.62E+00	2.26E+00	2.73E+00	2.18E+00	2.30E+00	2.39E+00	2.41E+00	3.04E+00	3.12E+00	2.48E+00	3.20E+00	2.91E+00

TABLE VIII: The complexity of the LSTM-based channel model.

	Prediction Time	0				1				2				3				4				5			
	Time Step	0	5	10	15	0	5	10	15	0	5	10	15	0	5	10	15	0	5	10	15	0	5	10	15
Blind Model	Training Time (s)	6.01E+00	1.51E+01	3.88E+01	7.86E+01	4.49E+00	1.60E+01	4.03E+01	8.22E+01	4.53E+00	1.65E+01	4.12E+01	8.54E+01	4.62E+00	1.74E+01	4.20E+01	8.57E+01	4.85E+00	1.80E+01	4.44E+01	9.19E+01	4.81E+00	1.86E+01	4.50E+01	8.45E+01
	Loading Time (s)	8.24E-02	1.56E-02	1.54E-02	1.30E-02	9.01E-03	1.56E-02	0.00E+00	1.57E-02	1.30E-02	0.00E+00	0.00E+00	1.53E-02	9.01E-03	1.54E-02	1.55E-02	0.00E+00	4.99E-03	1.55E-02	1.56E-02	4.66E-02	1.10E-02	1.54E-02	1.57E-02	1.57E-02
	Blind Prediction (s)	5.08E-01	6.40E-01	1.36E+00	2.20E+00	3.80E-01	6.72E-01	3.00E+00	2.39E+00	3.90E-01	6.87E-01	1.41E+00	2.39E+00	3.96E-01	7.50E-01	1.39E+00	2.33E+00	3.97E-01	7.19E-01	1.49E+00	2.36E+00	3.87E-01	7.34E-01	1.48E+00	2.25E+00
	Sunny Prediction (s)	1.38E-01	3.61E-01	9.22E-01	1.72E+00	1.37E-01	3.75E-01	9.69E-01	1.69E+00	1.50E-01	4.06E-01	9.53E-01	1.72E+00	1.44E-01	4.53E-01	9.69E-01	1.72E+00	1.51E-01	4.37E-01	9.69E-01	1.80E+00	1.57E-01	4.86E-01	1.02E+00	1.67E+00
	Rainy Prediction (s)	3.19E-02	6.22E-02	1.09E-01	2.05E-01	3.19E-02	4.68E-02	9.37E-02	2.03E-01	3.05E-02	6.21E-02	9.37E-02	1.56E-01	3.29E-02	4.69E-02	9.38E-02	1.90E-01	3.09E-02	6.22E-02	9.37E-02	2.66E-01	3.29E-02	6.25E-02	1.11E-01	2.50E-01
Sunny Model	Training Time (s)	4.42E+00	1.39E+01	3.57E+01	6.87E+01	4.24E+00	1.43E+01	3.72E+01	7.34E+01	4.66E+00	1.50E+01	3.80E+01	7.45E+01	4.44E+00	1.60E+01	3.89E+01	7.54E+01	5.63E+00	1.63E+01	3.94E+01	8.01E+01	5.03E+00	1.68E+01	4.12E+01	7.71E+01
	Loading Time (s)	8.98E-03	1.53E-02	1.53E-02	1.00E-02	9.97E-03	0.00E+00	1.53E-02	1.53E-02	9.97E-03	1.53E-02	1.53E-02	1.56E-02	1.10E-02	1.53E-02	1.53E-02	3.10E-02	8.95E-03	1.53E-02	1.53E-02	4.65E-02	8.98E-03	1.53E-02	1.53E-02	1.54E-02
	Blind Prediction (s)	3.80E-01	6.72E-01	1.28E+00	2.07E+00	3.82E-01	6.87E-01	1.27E+00	2.13E+00	3.84E-01	6.90E-01	1.28E+00	2.06E+00	4.08E-01	7.34E-01	1.31E+00	2.23E+00	3.88E-01	7.50E-01	1.30E+00	2.13E+00	8.17E-01	7.50E-01	1.42E+00	2.25E+00
	Sunny Prediction (s)	1.37E-01	3.92E-01	9.06E-01	1.56E+00	1.43E-01	3.91E-01	9.06E-01	1.69E+00	1.43E-01	4.22E-01	9.21E-01	1.63E+00	4.49E-01	4.53E-01	1.03E+00	1.80E+00	1.48E-01	4.53E-01	1.05E+00	1.61E+00	1.57E-01	4.53E-01	1.08E+00	1.73E+00
	Rainy Prediction (s)	3.09E-02	4.68E-02	9.37E-02	1.87E-01	3.19E-02	4.68E-02	9.37E-02	2.03E-01	3.29E-02	4.68E-02	1.25E-01	2.03E-01	3.30E-02	4.68E-02	1.09E-01	1.72E-01	3.19E-02	6.21E-02	1.09E-01	1.87E-01	3.19E-02	6.25E-02	1.09E-01	1.87E-01
Rainy Model	Training Time (s)	2.14E+00	2.73E+00	4.97E+00	8.29E+00	1.93E+00	2.75E+00	4.91E+00	8.67E+00	1.94E+00	2.84E+00	4.98E+00	8.73E+00	2.27E+00	4.08E+00	1.11E+01	9.98E+00	1.98E+00	2.92E+00	5.51E+00	9.23E+00	1.93E+00	2.95E+00	5.17E+00	9.09E+00
	Loading Time (s)	6.02E-03	1.53E-02	1.53E-02	1.53E-02	1.10E-02	1.67E-02	1.53E-02	0.00E+00	9.01E-03	1.53E-02	1.53E-02	1.53E-02	1.00E-02	1.53E-02	1.53E-02	1.53E-02	9.00E-03	1.53E-02	1.53E-02	1.53E-02	9.97E-03	0.00E+00	1.53E-02	1.54E-02
	Blind Prediction (s)	3.82E-01	6.72E-01	1.19E+00	2.16E+00	3.87E-01	6.72E-01	1.20E+00	2.05E+00	3.85E-01	6.87E-01	1.36E+00	2.02E+00	3.87E-01	7.20E-01	1.33E+00	2.11E+00	3.87E-01	7.19E-01	1.31E+00	2.08E+00	3.94E-01	1.81E+00	1.38E+00	2.05E+00
	Sunny Prediction (s)	1.32E-01	4.06E-01	8.45E-01	1.47E+00	1.44E-01	3.90E-01	9.84E-01	1.56E+00	1.39E-01	4.22E-01	9.68E-01	1.50E+00	1.45E-01	4.37E-01	9.53E-01	1.61E+00	1.53E-01	4.84E-01	9.53E-01	1.56E+00	1.41E-01	4.84E-01	9.84E-01	1.58E+00
	Rainy Prediction (s)	3.29E-02	4.68E-02	9.37E-02	1.56E-01	2.97E-02	6.21E-02	9.38E-02	2.34E-01	3.19E-02	4.69E-02	1.25E-01	2.19E-01	3.19E-02	4.69E-02	1.09E-01	2.03E-01	3.19E-02	6.25E-02	9.37E-02	2.34E-01	3.12E-02	4.68E-02	1.11E-01	2.19E-01

	Prediction Time	10				15				20				25				30				45				60			
	Time Step	0	5	10	15	0	5	10	15	0	5	10	15	0	5	10	15	0	5	10	15	0	5	10	15	0	5	10	15
Blind Model	Training Time (s)	5.58E+00	1.88E+01	4.65E+01	9.49E+01	5.14E+00	1.99E+01	6.05E+01	9.16E+01	5.14E+00	2.02E+01	4.97E+01	9.19E+01	6.06E+00	2.06E+01	4.88E+01	1.12E+02	5.78E+00	2.33E+01	5.10E+01	9.42E+01	6.25E+00	2.18E+01	5.24E+01	1.00E+02	6.27E+00	2.28E+01	5.28E+01	1.06E+02
	Loading Time (s)	1.57E-02	1.54E-02	1.54E-02	1.10E-02	0.00E+00	3.10E-02	1.60E-02	1.55E-02	0.00E+00	1.56E-02	1.56E-02	1.56E-02	0.00E+00	1.53E-02	1.53E-02	3.13E-02	1.53E-02	1.56E-02	1.56E-02	3.09E-02	1.56E-02	9.01E-03	1.56E-02	1.56E-02	1.56E-02	1.56E-02	1.54E-02	3.15E-02
	Blind Prediction (s)	3.90E-01	7.34E-01	1.52E+00	2.39E+00	4.06E-01	7.65E-01	1.62E+00	2.36E+00	4.22E-01	7.81E-01	1.53E+00	2.47E+00	4.14E-01	7.97E-01	1.58E+00	2.53E+00	4.22E-01	8.44E-01	6.59E+00	2.30E+00	4.06E-01	8.17E-01	1.58E+00	4.72E+00	4.37E-01	8.28E-01	1.59E+00	2.58E+00
	Sunny Prediction (s)	1.56E-01	5.00E-01	1.02E+00	1.83E+00	1.56E-01	5.15E-01	1.06E+00	1.72E+00	1.56E-01	5.31E-01	1.06E+00	2.02E+00	1.64E-01	5.31E-01	1.06E+00	1.83E+00	1.72E-01	5.33E-01	1.14E+00	1.72E+00	1.72E-01	5.67E-01	1.06E+00	1.87E+00	1.72E-01	5.47E-01	1.12E+00	2.02E+00
	Rainy Prediction (s)	3.12E-02	6.25E-02	1.40E-01	2.03E-01	3.12E-02	6.25E-02	1.25E-01	1.71E-01	3.13E-02	6.25E-02	1.09E-01	2.36E-01	3.29E-02	7.78E-02	1.25E-01	2.03E-01	4.65E-02	6.24E-02	1.25E-01	2.34E-01	4.65E-02	6.68E-02	1.09E-01	2.66E-01	4.65E-02	7.78E-02	1.09E-01	2.34E-01
Sunny Model	Training Time (s)	4.72E+00	1.73E+01	4.24E+01	8.16E+01	4.78E+00	1.82E+01	4.45E+01	8.14E+01	5.64E+00	1.88E+01	4.52E+01	9.04E+01	5.22E+00	1.95E+01	4.39E+01	8.76E+01	5.31E+00	1.99E+01	4.60E+01	8.38E+01	6.63E+00	2.00E+01	4.75E+01	9.40E+01	6.78E+00	2.05E+01	4.85E+01	9.33E+01
	Loading Time (s)	1.54E-02	0.00E+00	1.53E-02	1.53E-02	1.53E-02	1.53E-02	1.53E-02	1.53E-02	1.53E-02	1.53E-02	1.53E-02	1.53E-02	9.01E-03	1.53E-02	1.56E-02	3.13E-02	1.53E-02	1.53E-02	1.53E-02	1.53E-02	1.53E-02	9.97E-03	1.53E-02	1.53E-02	1.53E-02	0.00E+00	1.53E-02	1.54E-02
	Blind Prediction (s)	3.93E-01	7.81E-01	1.34E+00	2.17E+00	3.91E-01	7.81E-01	1.42E+00	2.25E+00	4.07E-01	7.81E-01	1.42E+00	2.30E+00	4.02E-01	8.15E-01	1.44E+00	2.26E+00	4.22E-01	7.81E-01	1.44E+00	2.33E+00	4.22E-01	8.34E-01	1.48E+00	2.41E+00	4.22E-01	8.12E-01	1.50E+00	2.50E+00
	Sunny Prediction (s)	1.56E-01	4.69E-01	1.06E+00	1.64E+00	1.71E-01	5.00E-01	9.69E-01	1.91E+00	1.71E-01	5.00E-01	1.06E+00	1.77E+00	1.64E-01	5.31E-01	1.03E+00	1.91E+00	1.71E-01	5.47E-01	1.06E+00	1.86E+00	1.72E-01	5.46E-01	1.25E+00	1.74E+00	1.87E-01	5.62E-01	1.05E+00	1.89E+00
	Rainy Prediction (s)	3.09E-02	6.25E-02	1.25E-01	1.72E-01	3.12E-02	6.25E-02	1.25E-01	2.50E-01	3.12E-02	6.25E-02	1.09E-01	2.19E-01	3.39E-02	6.25E-02	1.09E-01	2.50E-01	4.65E-02	6.59E-02	1.25E-01	1.72E-01	3.12E-02	6.25E-02	1.25E-01	2.66E-01	3.12E-02	7.78E-02	1.25E-01	1.87E-01
Rainy Model	Training Time (s)	2.06E+00	3.03E+00	5.61E+00	9.66E+00	1.97E+00	3.09E+00	5.56E+00	9.88E+00	1.92E+00	3.11E+00	5.84E+00	9.94E+00	2.02E+00	3.19E+00	5.94E+00	1.00E+01	2.78E+00	3.28E+00	6.25E+00	9.69E+00	2.02E+00	3.27E+00	5.76E+00	1.10E+01	2.08E+00	3.25E+00	6.10E+00	1.08E+01
	Loading Time (s)	0.00E+00	1.53E-02	1.53E-02	1.53E-02	1.53E-02	1.53E-02	1.56E-02	1.53E-02	1.53E-02	1.53E-02	1.53E-02	1.53E-02	9.00E-03	1.54E-02	1.53E-02	1.53E-02	1.53E-02	9.01E-03	1.53E-02	1.53E-02	1.53E-02	1.53E-02	1.53E-02	8.98E-03	1.56E-02	1.53E-02	1.53E-02	1.53E-02
	Blind Prediction (s)	4.06E-01	7.65E-01	1.45E+00	2.08E+00	4.06E-01	7.81E-01	1.49E+00	2.24E+00	4.06E-01	7.68E-01	1.72E+00	2.14E+00	4.12E-01	7.83E-01	1.37E+00	2.33E+00	1.06E+00	8.34E-01	1.36E+00	2.30E+00	4.22E-01	7.97E-01	1.58E+00	2.70E+00	4.06E-01	8.28E-01	1.49E+00	2.95E+00
	Sunny Prediction (s)	1.58E-01	4.71E-01	1.02E+00	1.62E+00	1.56E-01	5.00E-01	1.08E+00	1.98E+00	1.71E-01	5.31E-01	1.12E+00	1.69E+00	1.56E-01	4.87E-01	1.02E+00	1.86E+00	1.72E-01	5.25E-01	9.71E-01	1.74E+00	1.72E-01	5.47E-01	1.11E+00	1.75E+00	1.72E-01	5.31E-01	1.22E+00	2.14E+00
	Rainy Prediction (s)	4.69E-02	4.69E-02	1.09E-01	1.87E-01	3.12E-02	6.25E-02	1.09E-01	3.29E-01	3.12E-02	6.25E-02	1.25E-01	2.03E-01	3.12E-02	6.25E-02	1.25E-01	1.72E-01	3.12E-02	6.48E-02	1.09E-01	1.87E-01	3.12E-02	6.25E-02	1.41E-01	1.87E-01	3.12E-02	7.78E-02	1.25E-01	2.34E-01

[15] S. Ventouras, R. Reeves, E. Rumi, F.P. Fontan, F. Machado, V. Pastoriza, A.Rocha, S. Mota, F. Jorge, A. D. Panagopoulos, A. Z. Papafragkakis, C. I. Kourogiorgas, O. Fiser, V. Pek, P. Pesice, M. Grabner, A. Vilhar, A. Kelmendi, A. Hrovat, D. Vanhoenacker-Janvier, L. Quibus, G.Goussetis, A. Coutsouris, J. Nessel, and A. Martellucci, "Assessment of spatial and temporal properties of Ka/Q-band earth-space radio channel across Europe using ALPHASAT TDP5," *International Journal of Satellite Communications and Networking*, vol. 37, no. 5, pp. 477–501, Jun. 2019.

[16] L. Bai, C.-X. Wang, G. Goussetis, S. Wu, Q. Zhu, W. Zhou, and E.-H. M. Aggoune, "Channel modeling for satellite communication channel at Q-band in high latitude," *IEEE Access*, vol. 7, pp. 137691–137703, Sept. 2019.

[17] H. Fenech, A. Tomatis, S. Amos, J. S. Merino, and V. Soumpholphakdy, "An operators perspective on propagation," in *Proc. IEEE EUCAP'14*, The Hague, Netherlands, Apr. 2014, pp. 2164–3342.

[18] A. Panagopoulos, P. Arapoglou, and P. Cottis, "Satellite communications at Ku, Ka, and V-bands: Propagation impairments and mitigation techniques," *IEEE Communications Surveys & Tutorials*, vol. 6, no. 3, pp. 2–14, Oct. 2004.

[19] 3GPP, R1-1805083, "Modeling of tropospheric scintillation effects in NTN channel model," InterDigital Inc., 3GPP TSG RAN WG1 Meeting #92bis, Sanya, China, April , 2018.

[20] ITU-R P.840-7, "Attenuation due to clouds and fog", Sept. 2017.

[21] X. Cheng, Z. Huang, and S. Chen, "Vehicular communication channel measurement, modeling, and application for B5G and 6G," *IET Communications*, accepted.

[22] L. Bai, C.-X. Wang, G. Goussetis, Q. Xu, and S. Ventouras, "Prediction of channel excess attenuation for satellite communication systems at Q-band using artificial neural network," *IEEE Antennas and Wireless Propaga. Lett.*, vol. 18, no. 11, pp. 2235–2239, Nov. 2019.

[23] X. Cheng, Y. Li, C-X. Wang, X. Yin, and D. W. Matolak, "A 3D geometry-based stochastic model for unmanned aerial vehicle MIMO Ricean fading channels," *IEEE Internet of Things Journal*, pp. 1–1, May, 2020, Early Access.

[24] G. Karam and H. Sari, "A data pre-distortion technique with memory for QAM radio systems," *IEEE Trans. Commun.*, vol. 39 no. 2, pp. 336–344, Feb. 1991.

[25] B. Li, C. Zhao, M. Sun, H. Zhang, Z. Zhou, and A. Nallanathan, "A Bayesian approach for nonlinear equalization and signal detection in millimeterwave communications," *IEEE Trans. Wireless Commun.*, vol. 14, no. 7, pp. 3794–3809, Jul. 2015.

[26] L. Bai, C.-X. Wang, J. Huang, Q. Xu, Y. Yang, G. Goussetis, J. Sun, and W. Zhang, "Predicting wireless mmWave massive MIMO channel characteristics using machine learning algorithms," *Wireless Commun. Mobile Computing*, vol. 2018, Article ID 9783863, https://doi.org/10.1155/2018/9783863, Aug. 2018.

[27] Agnew, J. (2013): Chilbolton Facility for Atmospheric and Radio Research (CFARR) Campbell Scientific PWS100 present weather sensor data. NCAS British Atmospheric Data Centre, Apr. 2020. https://catalogue.ceda.ac.uk/uuid/e490cd13d86d832bd2d62f1650d7b265

[28] Science and Technology Facilities Council, Chilbolton Facility for Atmospheric and Radio Research, Natural Environment Research Council, Wrench, C.L. (2003): Chilbolton Facility for Atmospheric and Radio Research (CFARR) Meteorological Sensor Data, Chilbolton Site. NCAS British Atmospheric Data Centre, Apr. 2020. https://catalogue.ceda.ac.uk/uuid/45b25a7c531563f4422afcaeea0f07a7

[29] Science and Technology Facilities Council, Chilbolton Facility for Atmospheric and Radio Research, Natural Environment Research Council, Wrench, C.L. (2003): Chilbolton Facility for Atmospheric and Radio Research (CFARR) Multiple Raingauges Data, Chilbolton Site. NCAS British Atmospheric Data Centre, Apr. 2020. https://catalogue.ceda.ac.uk/uuid/614747245770927bbe7565b690945ec3

[30] Science and Technology Facilities Council, Chilbolton Facility for Atmospheric and Radio Research, Natural Environment Research Council, Wrench, C.L. (2003): Chilbolton Facility for Atmospheric and Radio Research (CFARR) Meteorological Sensor Data, Chilbolton Site. NCAS British Atmospheric Data Centre, Apr. 2020. https://www.chilbolton.stfc.ac.uk/Pages/home.aspx

[31] X. Glorot and A. Bordes, "Deep sparse rectifier neural networks," *Journal of Machine Learning Research*, vol. 15, pp. 315–323, 2011.

[32] Keras Document, https://keras.io/

[33] S. Ruder, "An overview of gradient descent optimization algorithms," *arXiv preprint arXiv:1609.04747v2*, 2016.

[34] X. Glorot and Y. Bengio, "Understanding the difficulty of training deep feedforward neural networks," *Journal of Machine Learning Research*, vol. 9, pp. 249–256, 2010.

[35] S. Hochreiter and J. Schmidhuber, "Long short-term memory," *Neural Computation*, vol. 9, no. 8, pp. 1735–1780, 1997.

[36] Keras Document, https://keras.io/

[37] X. Glorot and Y. Bengio, "Understanding the difficulty of training deep feedforward neural networks," *Journal of Machine Learning Research*, vol. 9, no. 1, pp. 249—256, 2010.

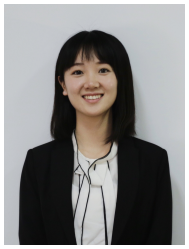

Lu Bai received the Ph.D. degree in Information and Communication Engineering from Shandong University, China, in 2019. From 2017 to 2019, she was also a visiting Ph.D. student at Heriot-Watt University, UK. Now, she is a research fellow at Beihang University, China. Her research interests is (B)5G wireless communication channel measurements and modeling, including massive MIMO channel measurements and modeling, satellite-terrestrial integrated communication channel modeling, and machine learning based channel modeling.

Qian Xu received the B.S. and M.S. degrees in software engineering from Jilin University, where he is currently pursuing the Ph.D. degree in computer application technology. His research interests include object detection and image segmentation.

Shangbin Wu received his B.Sc. degree in Communication Engineering from South China Normal University, Guangzhou, China, in 2009, M.Sc. degree in Wireless Communications with distinction from University of Southampton, Southampton, UK, in 2010, and Ph.D. degree in Electrical Engineering from the Heriot-Watt University, Edinburgh, UK in 2015. From 2010 to 2011, he worked as a LTE R&D engineer responsible for LTE standardization and system level simulation in New Postcom Equipment Ltd., Guangzhou, China. From October 2011 to August 2012, he was with Nokia Siemens Network, where he worked as a LTE algorithm specialist, mainly focusing on LTE radio resource management algorithm design and system level simulations. He has been with Samsung R&D Institute UK as a 5G researcher since November 2015.

George Goussetis [S'99, M'02, SM'12] received the Diploma degree in Electrical and Computer Engineering from the National Technical University of Athens, Greece, in 1998, and the Ph.D. degree from the University of Westminster, London, UK, in 2002. In 2002 he also graduated B.Sc. in physics (first class) from University College London (UCL), UK. In 1998, he joined the Space Engineering, Rome, Italy, as RF Engineer and in 1999 the Wireless Communications Research Group, University of Westminster, UK, as a Research Assistant. Between 2002 and 2006 he was a Senior Research Fellow at Loughborough University, UK. He was a Lecturer (Assistant Professor) with Heriot-Watt University, Edinburgh, UK between 2006 and 2009 and a Reader (Associate Professor) with Queen's University Belfast, UK, between 2009 and 2013. In 2013 he joined Heriot-Watt as a Reader and was promoted to Professor in 2014, where he currently directs the Institute of Sensors Signals and Systems. He has authored or co-authored over 500 peer-reviewed papers five book chapters one book and four patents. His research interests are in the area of microwave and antenna components and subsystems. Dr. Goussetis has held a research fellowship from the Onassis foundation in 2001, a research fellowship from the UK Royal Academy of Engineering between 2006–2011 and European Marie-Curie experienced researcher fellowships in 2011–12 and again in 2014–17. He is the co-recipient of the 2011 European Space Agency young engineer of the year prize, the 2011 EuCAP best student paper prize, the 2012 EuCAP best antenna theory paper prize and the 2016 Bell Labs prize. He has served as Associate Editor to the IEEE Antennas and Wireless Propagation Letters.